30th IEA-TLM in Capri

群馬大学
GUNMA UNIVERSITY

Subtask 1.4G: Investigate Combustion in Premixed Charge Spark/Compression Ignition Engines

Turbulence Characteristics in the Cylinder Flow of a 4-stroke Motored Engine by Means of LDA

*** Tomio OBOKATA, Masaaki KATO and Tsuneaki ISHIMA**
Department of Mechanical System Engineering, Gunma University
1-5-1 Tenjin, Kiryu, Gunma 376-8515, Japan
Makoto KANEKO
Fuji Heavy Industries Ltd.
3-9-6, Osawa, Mitaka-shi, Tokyo 181-8577, Japan

BACK GROUND

It is requested for I.C. engine to improve the thermal efficiency
with satisfying the exhaust emission regulations.

To understand and control the gas flows in the cylinder is the key technology
for improving the I.C. engine.
However, it is not easy to understand the turbulence characteristics of gas flows
because they are intermittent, highly turbulent
and 3-dimensional complex flows.

Recently, numerical simulations of gas flow and combustion (CFD) are
important and powerful tools to understand the gas flows in the cylinder.

But, it is important to verify the CFD results
by the reliable and detailed experimental data obtaining at the same engine.

PURPOSE

- Many research groups in RC226(Prof.Moriyoshi) and RC238 (Prof. Tomita) of JSME are performing the numerical simulation of in-cylinder flow using the same engine specifications with different numerical simulation codes such as STAR-CD, VECTIS, Fluent and so on. It is like a competition.

- Our experiment group in the same RCs of JSME are preparing a reliable database on the turbulent characteristics of in-cylinder flows at the same engine by LDA and PIV for verifying the numerical results.

- Turbulent characteristics of gas flow in the I.C. engine are also analyzing experimentally under various operating conditions. Comparison between motoring and firing operations will be expected near future.

EXPERIMENTAL SETUP

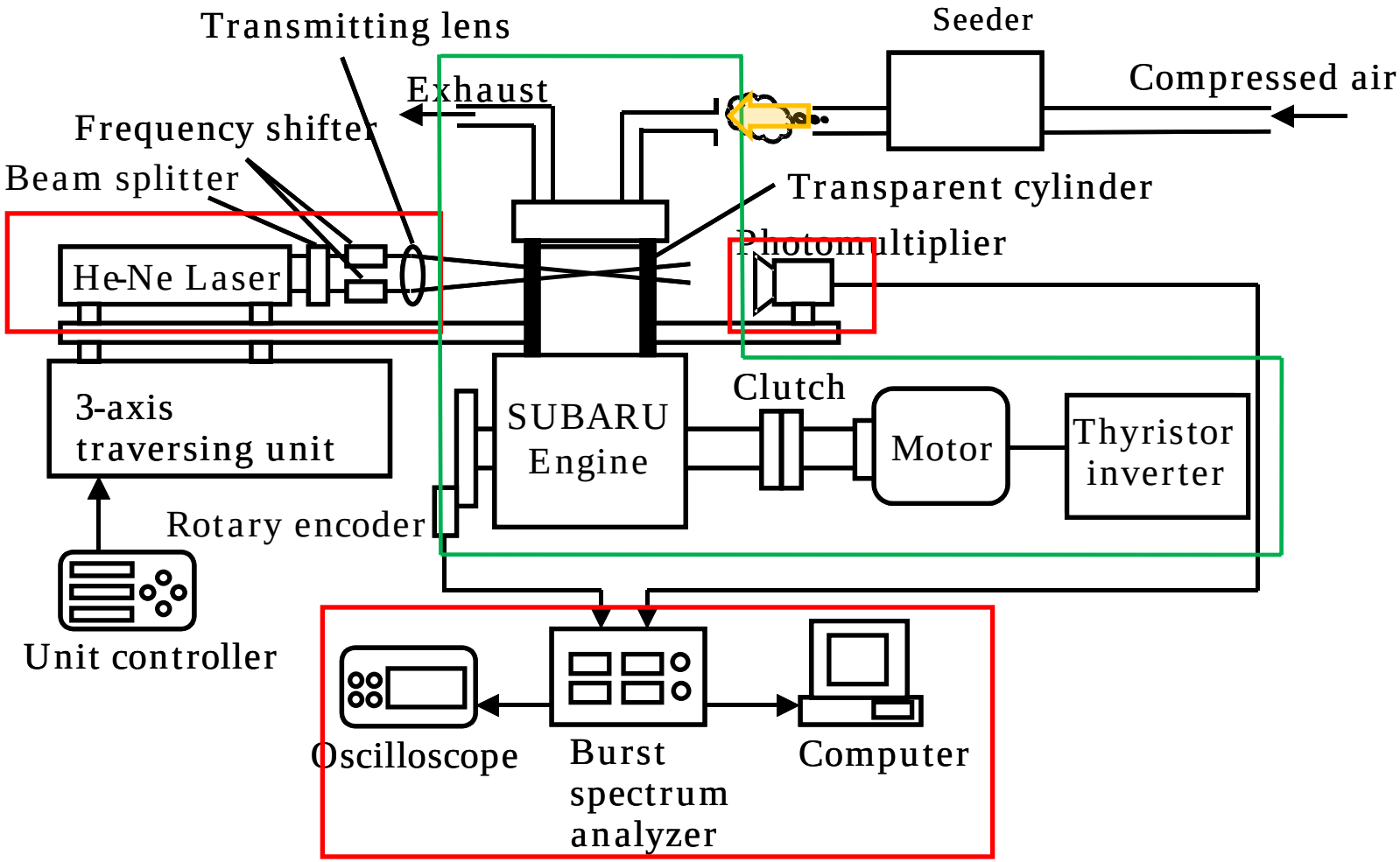

- Apparatus for this experiment divided into components of the optical system and the motored engine.
- Tracer particles are added in the intake airflow before the intake port.

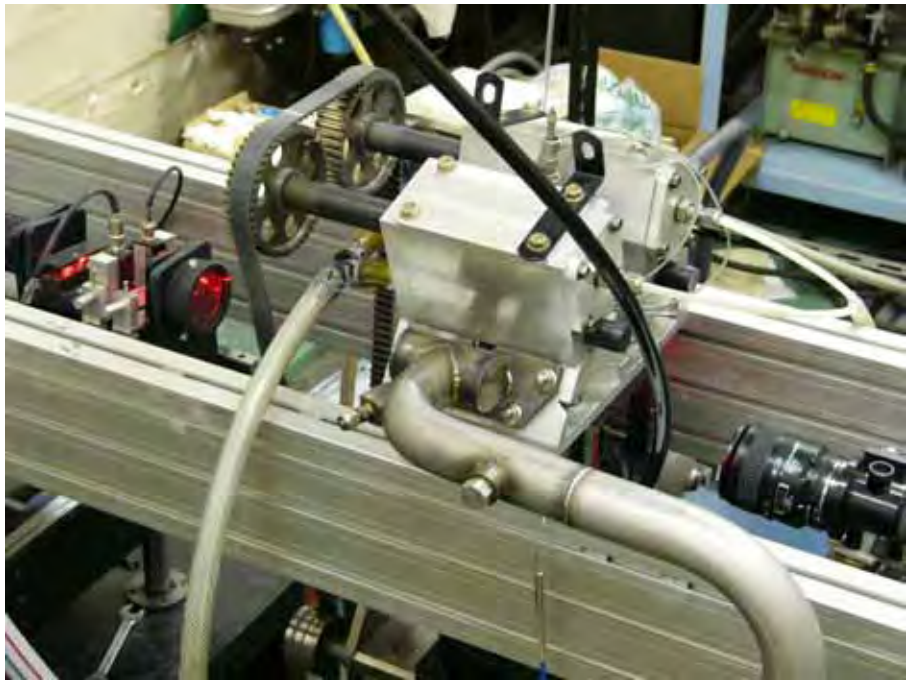

Specifications of LDA

Wave length	632.8 nm
Beam separation	50 mm
Beam diameter	1.35 mm
Focal length	300 mm
Full beam cross angle	9.52 °
Calibration factor	3.81 m/s/MHz
Diameter of waist	179 μm
Measuring volume length	2.26 mm
Measuring volume width	179 μm
Shift frequency	10 MHz

A conventional 1-compornent LDA is used in this measurement.

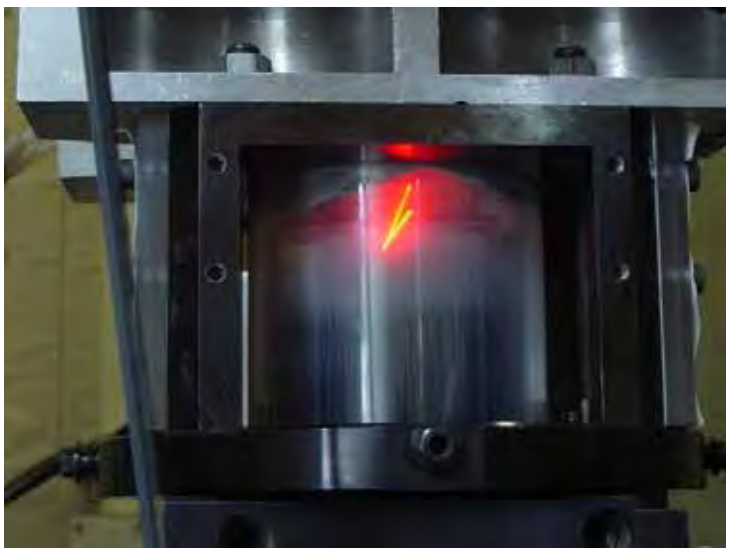

TiO_2 (KURONOS TITAN 2220)

Mean particle size	0.4 μm
Density	4.0 g/cm^3
Apparent relative density	900 kg/m^3

SiO_2 (Degussa AEROSIL R812)

Mean particle size	7 nm
Density	2.2 g/cm^3
Apparent relative density	50 kg/m^3

Titanium dioxide is used for the tracer particle.
For decrease in the effect of the humidity, silicone dioxide is added.

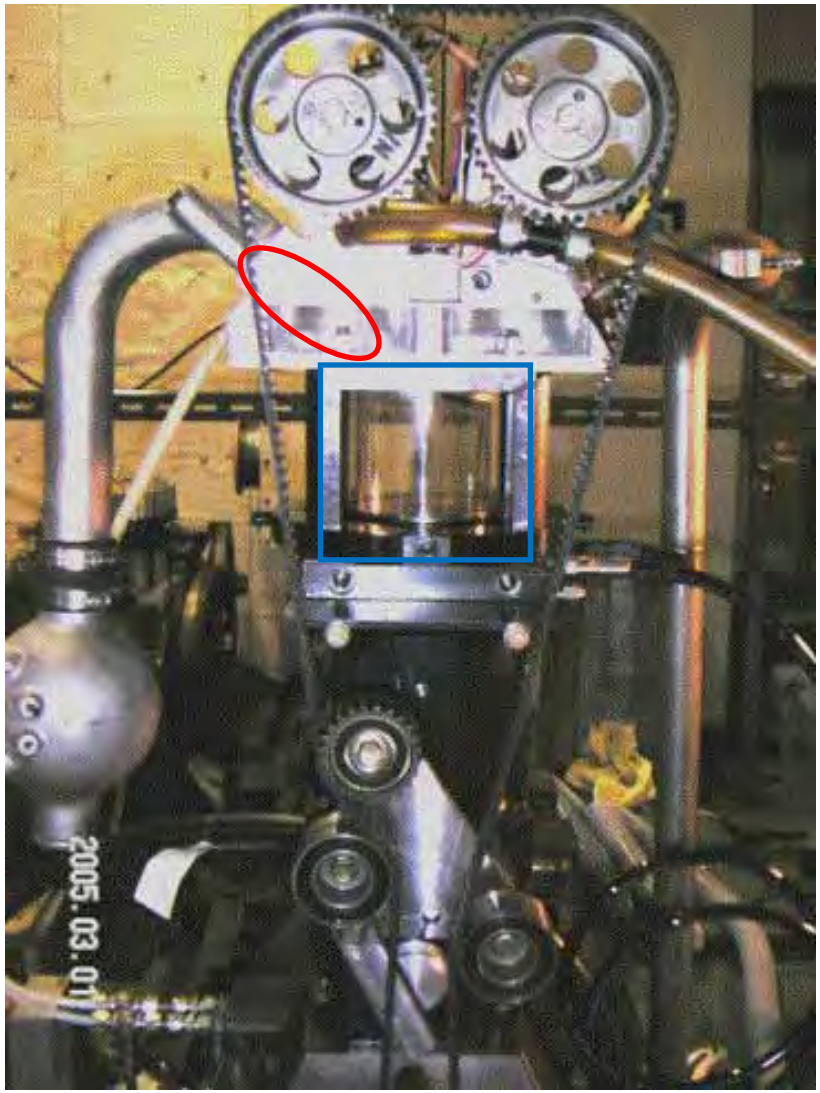

Specifications of SUBARU test engine

Engine type	4-stroke, Single cylinder
Combustion chamber	Pentroof type
Bore × Stroke	96.9 mm×74 mm
Displacement	545.7 cc
Compression ratio	11.5
Intake valve opening	4 deg.
Intake valve closure	240 deg.
Exhaust valve opening	485 deg.
Exhaust valve closure	5 deg.

The cylinder of this engine is made by sapphire for optical measurement.

This engine has a tumble generation valve.
The in-cylinder flow structure is changed by the cases of with and without the valve.

Operating condition

Motoring	600rpm
TGV	With TGV / Without TGV

※Tumble Generation Valve (TGV)

The motoring condition is sets with 600 rpm of engine speed in the measurement.

Prototype Tumble Generation Valve (TGV)

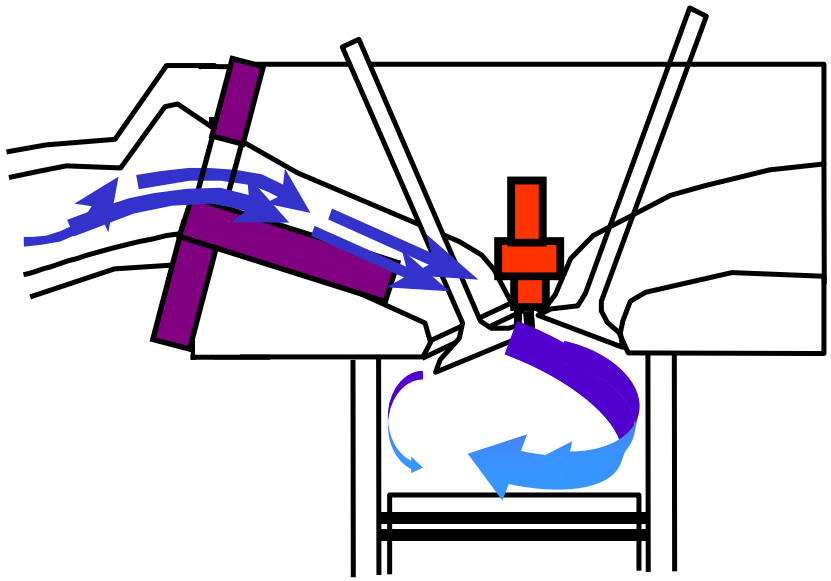

When the case of without TGV, half cylindrical structures of the TGV are removed.

ne.

half of the intake port.

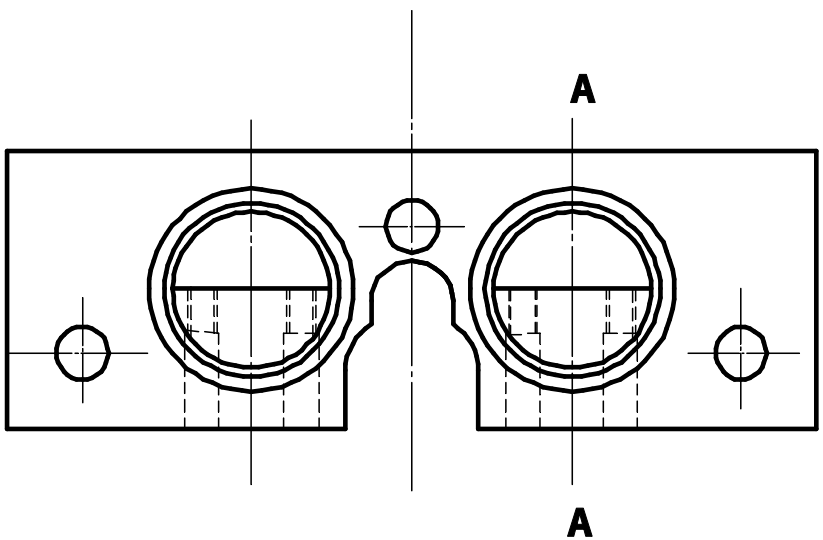

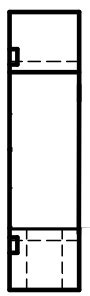

A-A

Result 1 Measurement of flow velocity through a intake valve.

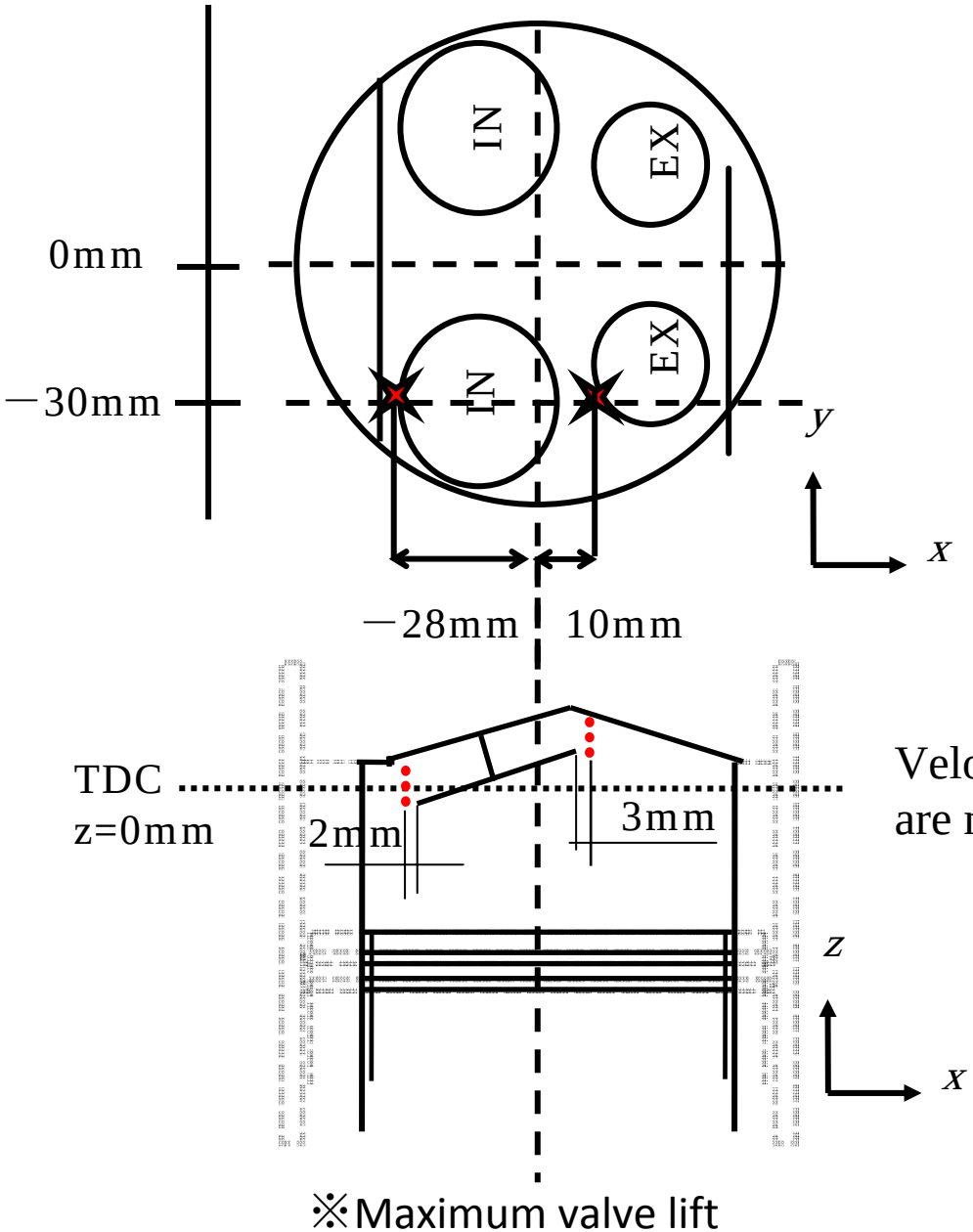

Measure point

x,y =10,-30mm	z =9,7,4mm
x,y =-28,-30mm	z =2,0,-2mm

Velocities from the intake valve at some points are measured with and without TGV conditions.

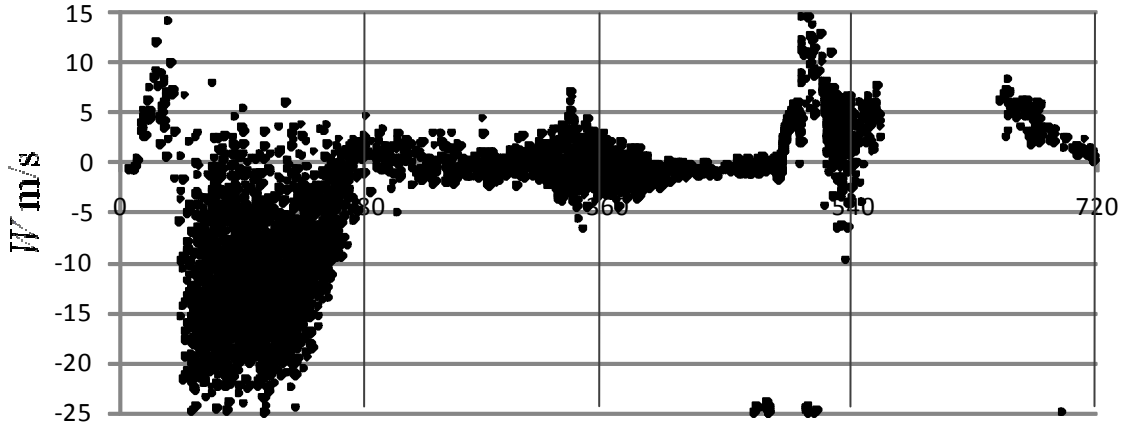

Crank angle degree

Ensemble instantaneous velocity through a valve

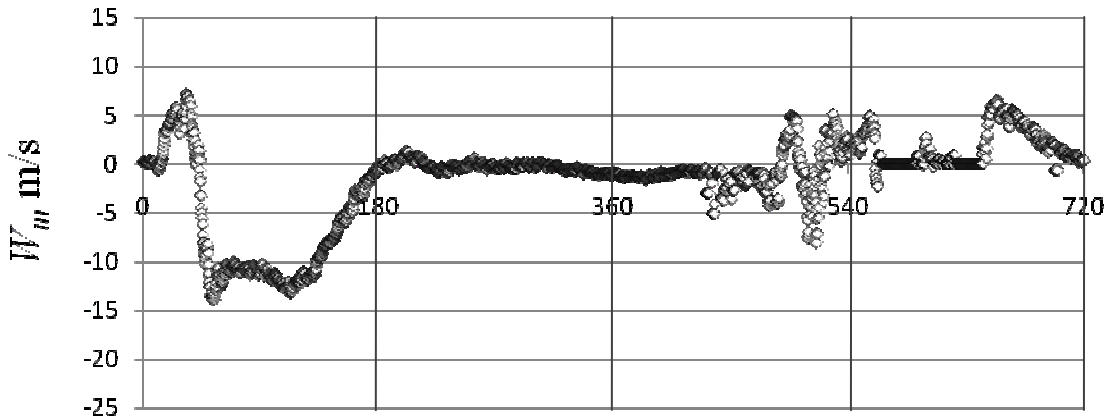

Crank angle degree

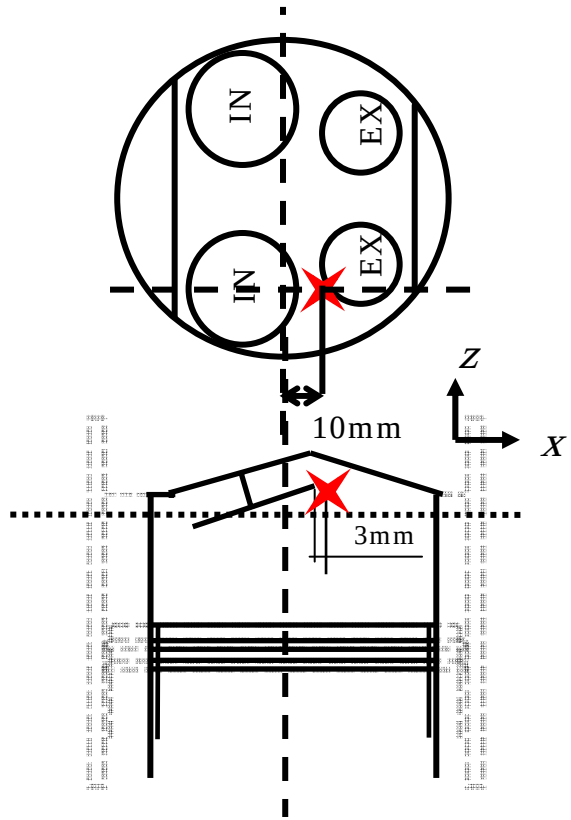

Ensemble averaged mean velocity through a valve $\triangle \theta$:0.25deg.

Examples of ensemble axial velocity through a valve
at x=10 mm y= - 30 mm z=4 mm with TGV.

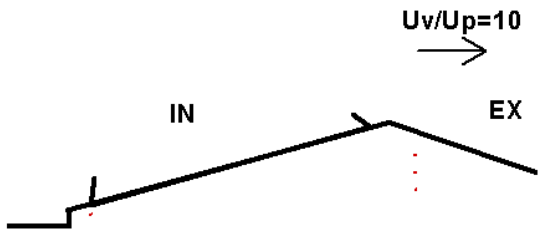

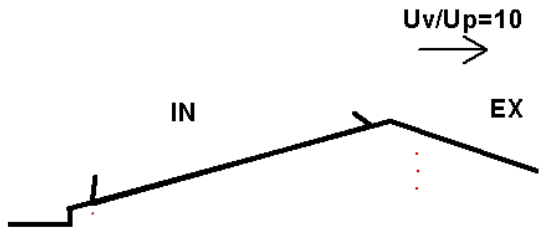

Without TGV

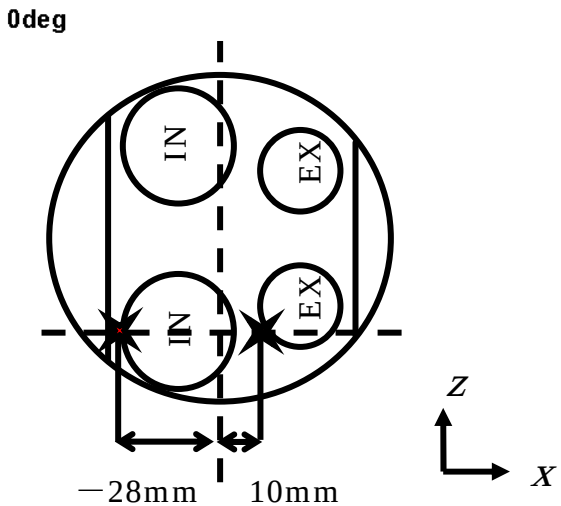

With TGV

0deg

Animations of the flow velocity through a valve

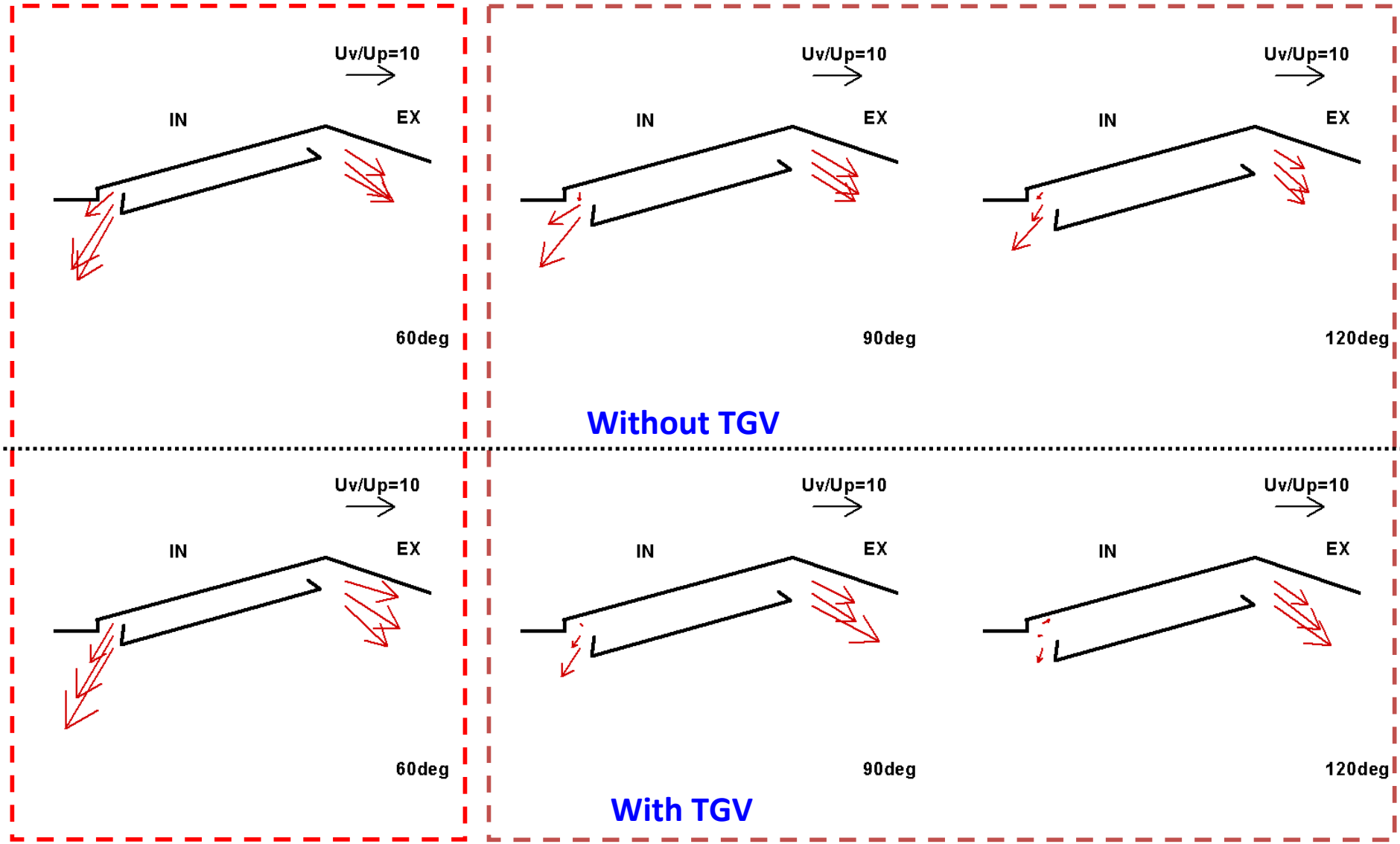

At 90 degree of the crank angle, the velocity at the right hand side with TGV becomes larger than that of without TGV case.
The difference in the left hand side is more remarkable than that of the right hand side.
At the 120 degree of the crank angle, the velocity tendencies are almost same with that of the 90 degree of crank angle.

Flow velocity through a valve at 60,90,120deg.

Result 2 Measurement of in-cylinder flow velocity .

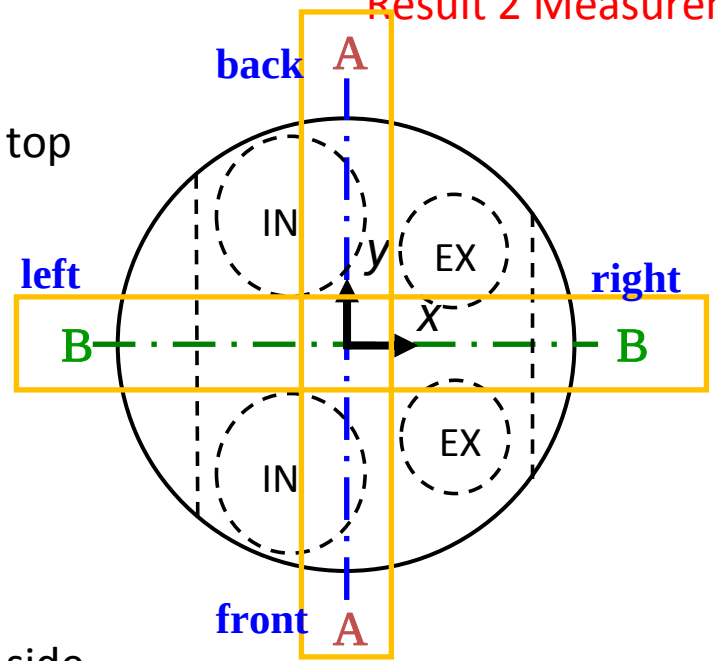

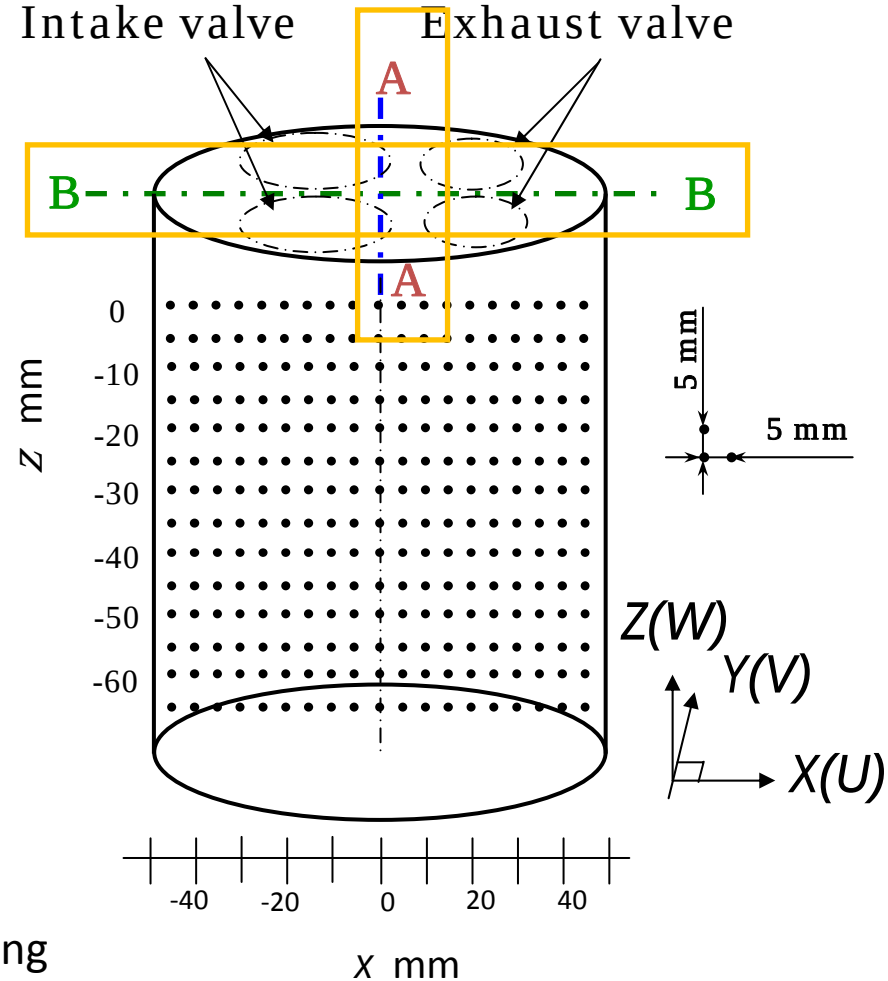

50,000 samples are obtained at all of the measurement points.

A-A plane is the section from front side to back side and is set to Y-Z plane.

The velocity of cylinder and swirl directions on the A-A and B-B planes are measured.
The instantaneous velocity components of *U*, *V* and *W* are directed to *x*, *y* and *z*.

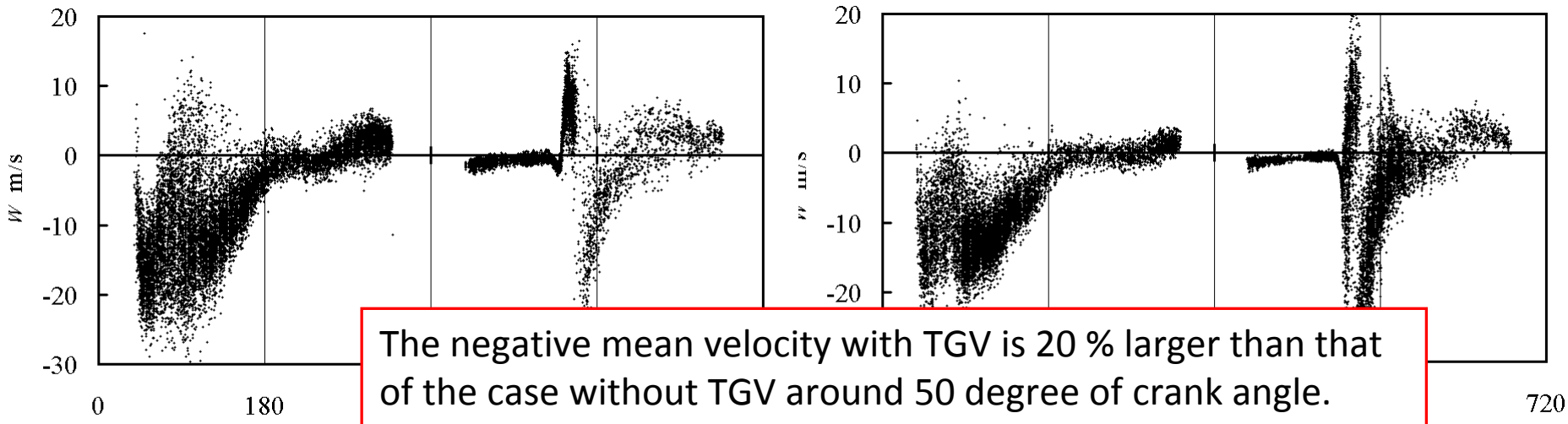

The negative mean velocity with TGV is 20 % larger than that of the case without TGV around 50 degree of crank angle.
The fluctuating intensity w_{rms} with TGV is also larger than that of without TGV case at the same crank angle.

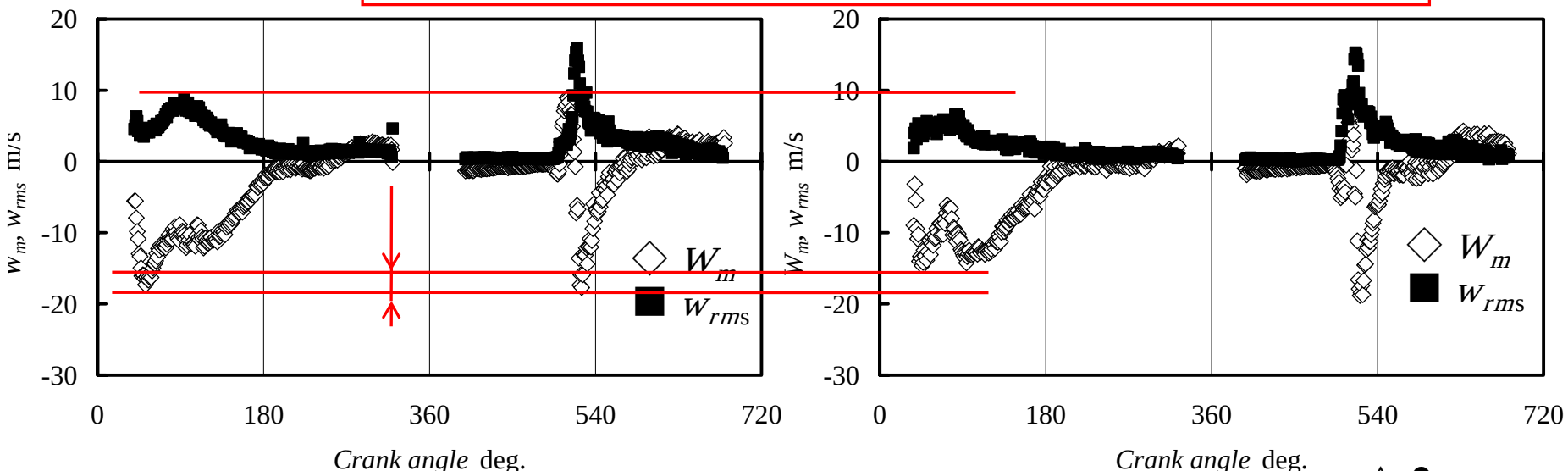

With TGV

Without TGV

△ θ :0.25deg.

Ensemble averaged mean velocity and fluctuating intensity

Examples of axial velocity data (x,y,z = 0,0,-10mm)

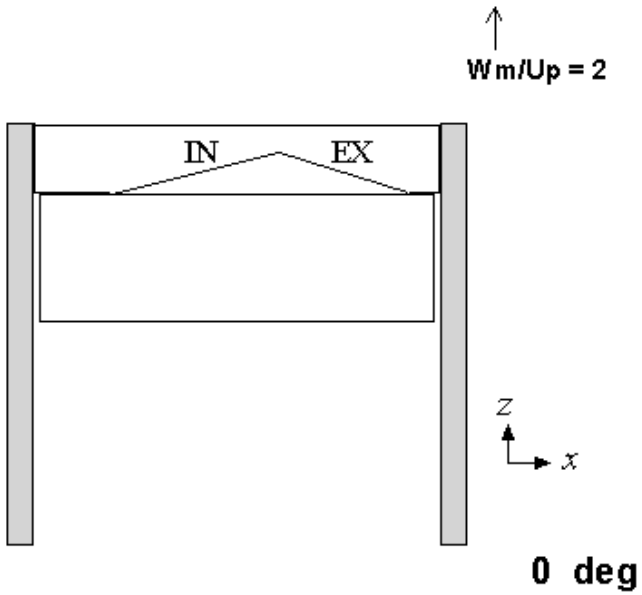

B-B

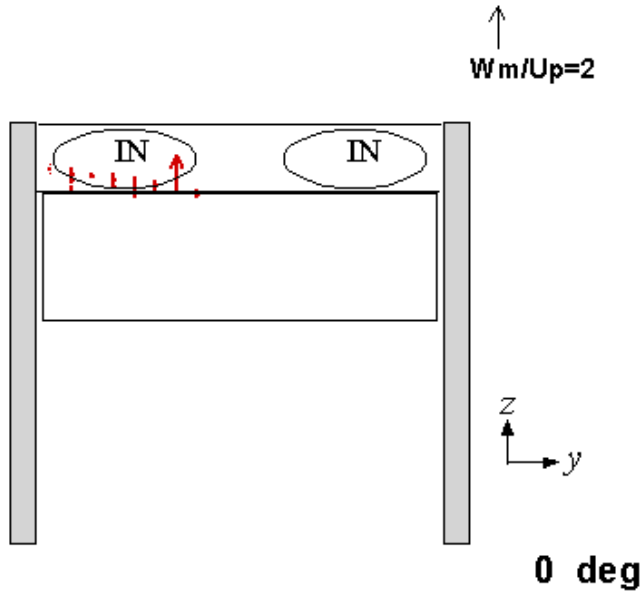

A-A

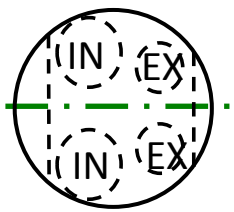

Front View

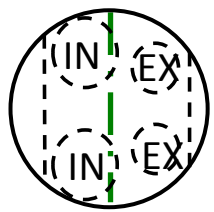

Side View

The velocities are normalized by the mean piston velocity

Animation of the ensemble averaged velocity distributions of Wm at vertical section of B - B and A - A with TGV

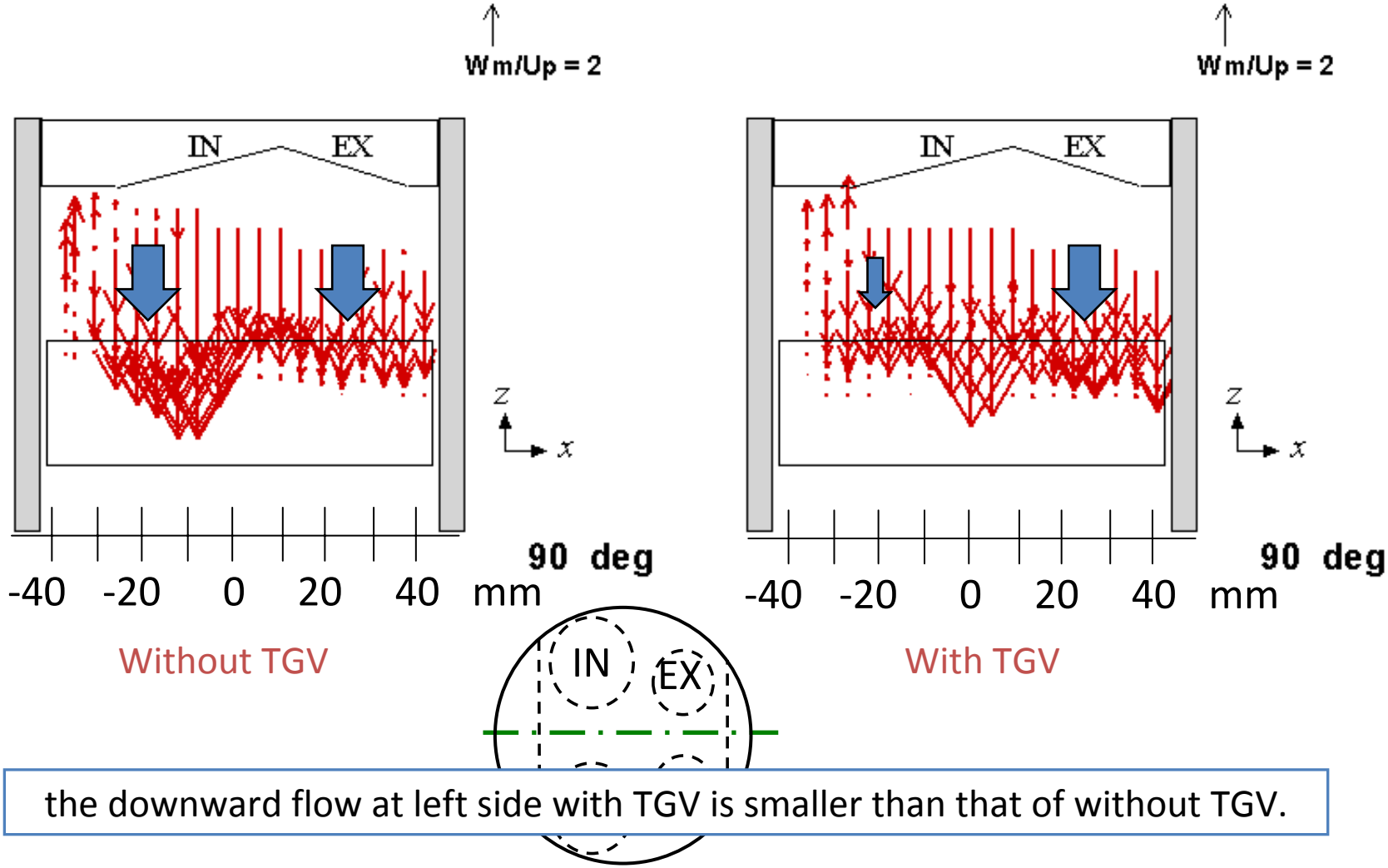

the downward flow at left side with TGV is smaller than that of without TGV.

Ensemble averaged velocity distributions of W_m in the vertical section at 90deg.

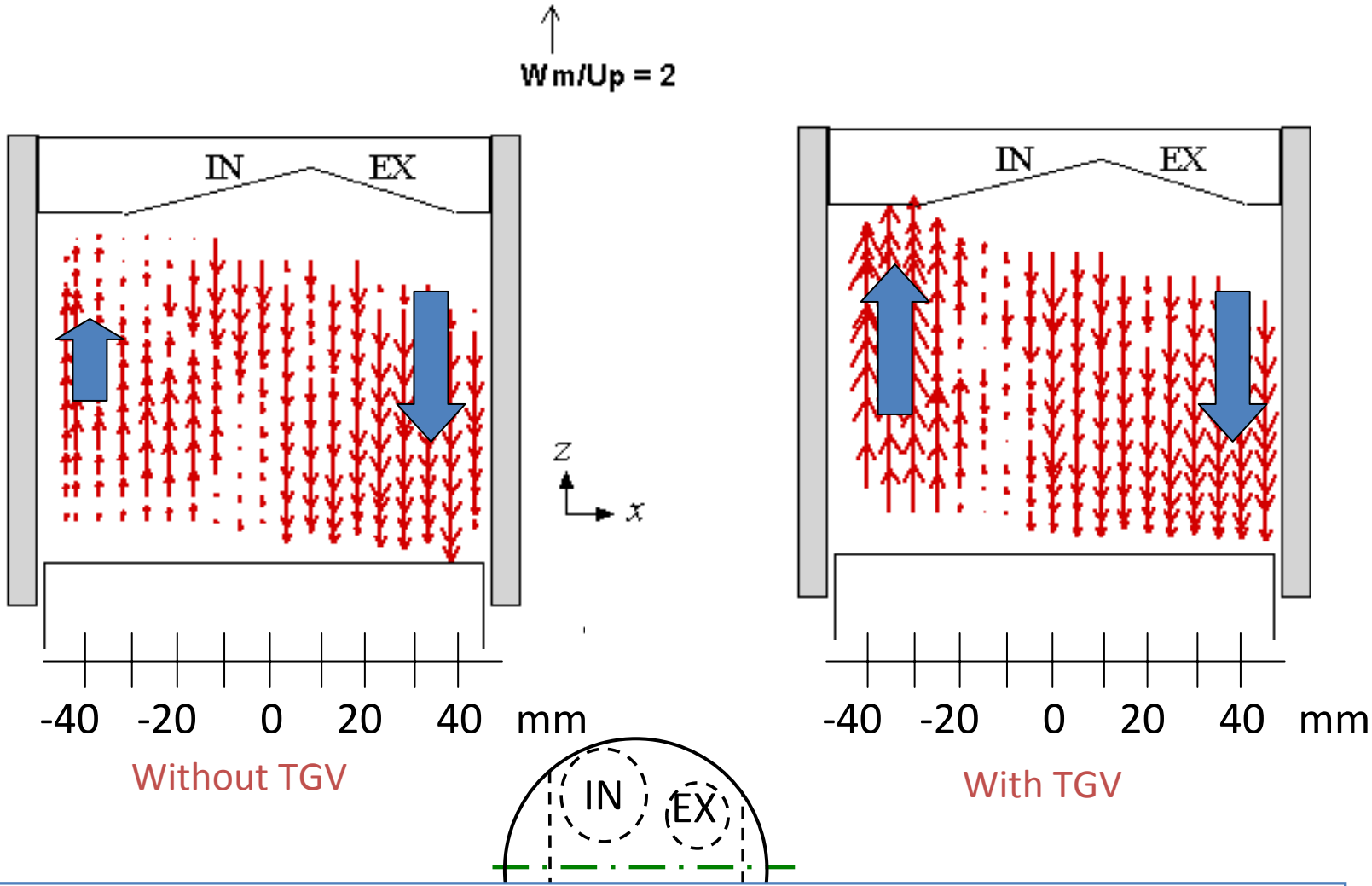

The results indicate the strong tumble motion with TGV condition.
The upward flow at left side is not disturbed by the flow from the intake valve.

Ensemble averaged velocity distributions of W_m in the vertical section at 180deg.

Example of comparison between CFD result and experiment

- Vector maps of in-cylinder flow are performed by using the simulation code of STAR-CD.
- Lines show the mean axial velocity distributions by the simulation and marked lines show the mean velocity distributions by the experiment.

This figure was made by Dr. Makoto KANEKO

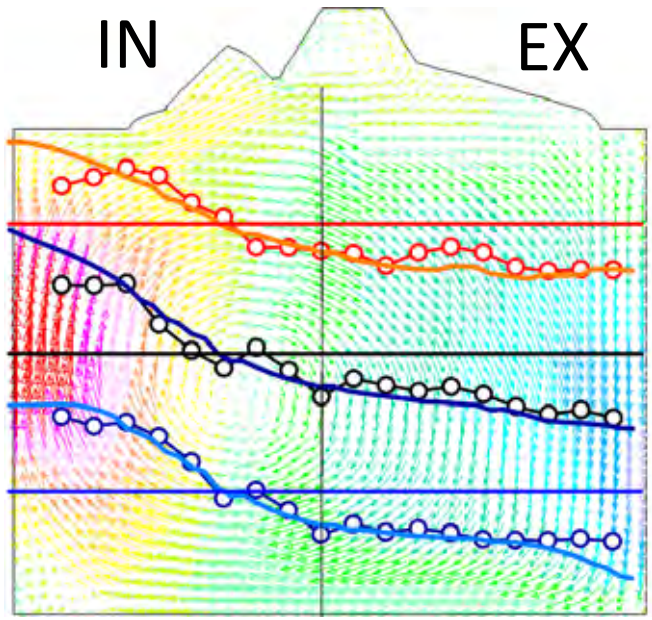

B-B Plane

Simulation results are in excellent agreement with experimental results in points of mean velocity distributions and center of the tumble rotation.

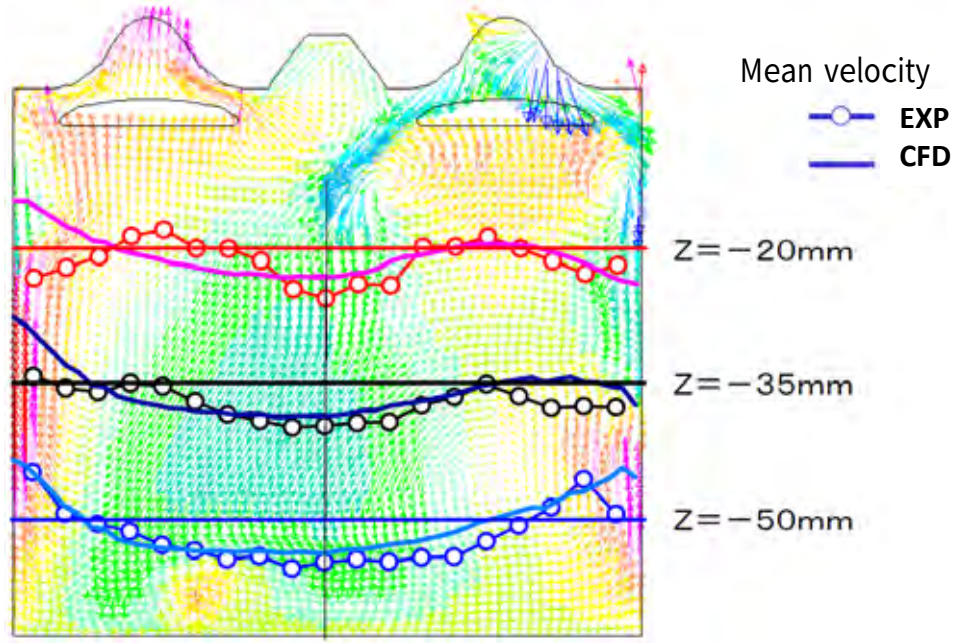

A-A Plane

The mainstream on this plane of the simulation result is coincident with that of the experiment.

Axial velocity distributions of A-A and B-B section at 180degree with TGV.

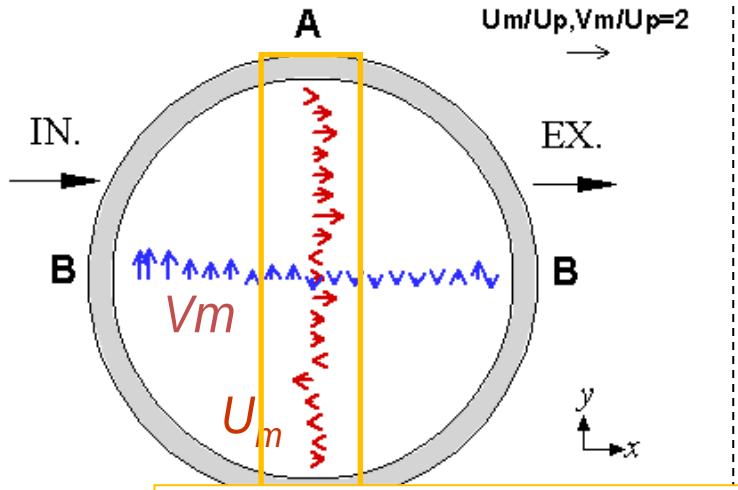

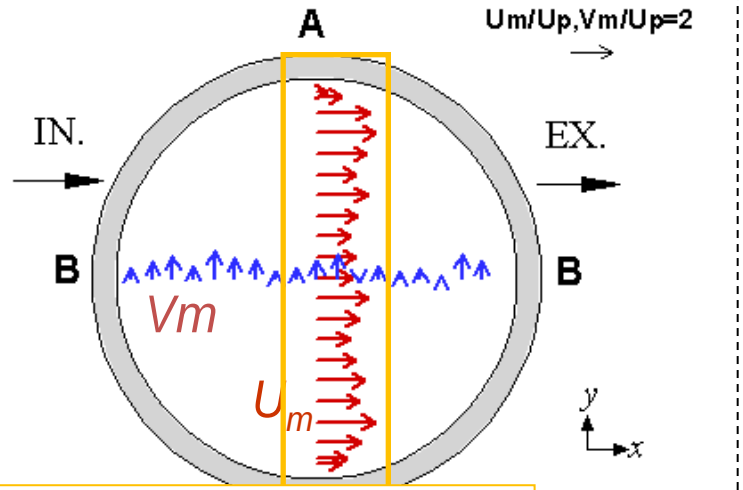

Magnitudes of the velocities U_m with TGV is lager than that of without TGV at the upper side.

180 deg

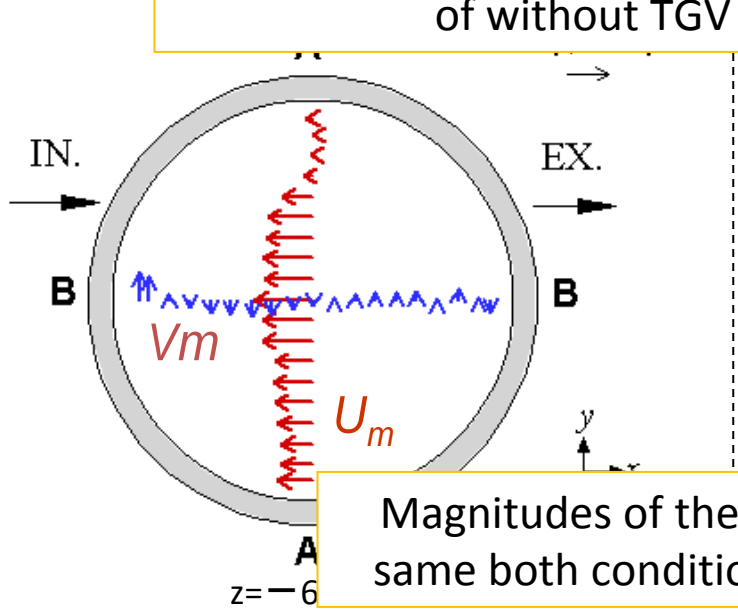

Without TGV

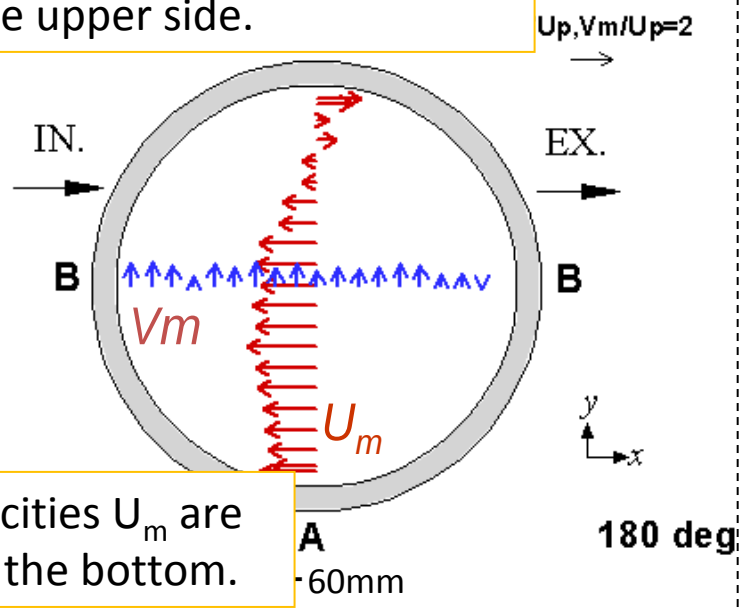

With TGV

Magnitudes of the velocities U_m are same both condition at the bottom.

180 deg

The effect of the TGV at upper side of the cylinder become large compared with lower side of the cylinder.

Ensembl

0deg.

Example of comparison between CFD result and experiment

- Vector maps of in-cylinder flow are performed by using the simulation code of STAR-CD.
- Lines show the mean swirl direction velocity distributions by the simulation and marked lines show the mean velocity distributions by the experiment.

This figure was made by Dr. Makoto KANEKO

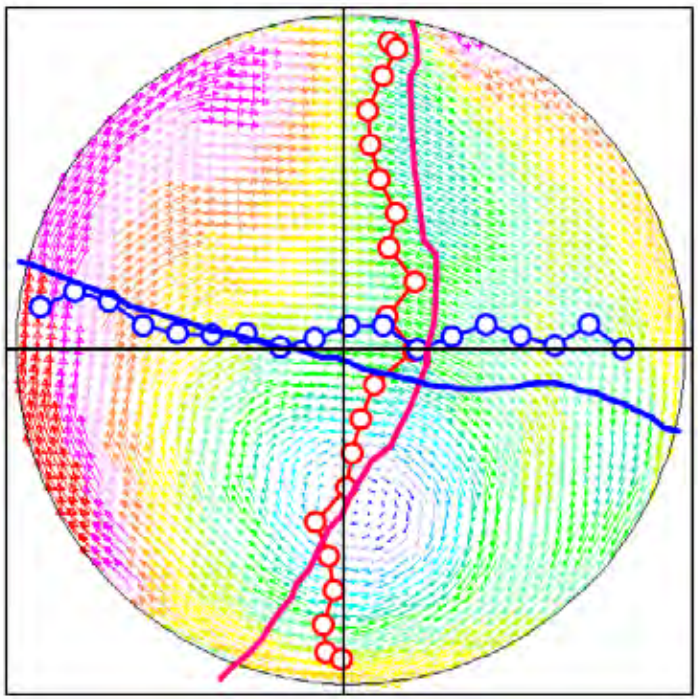

Z=-20 mm

Velocity distributions of simulation are roughly coincident with the result of the experiment.

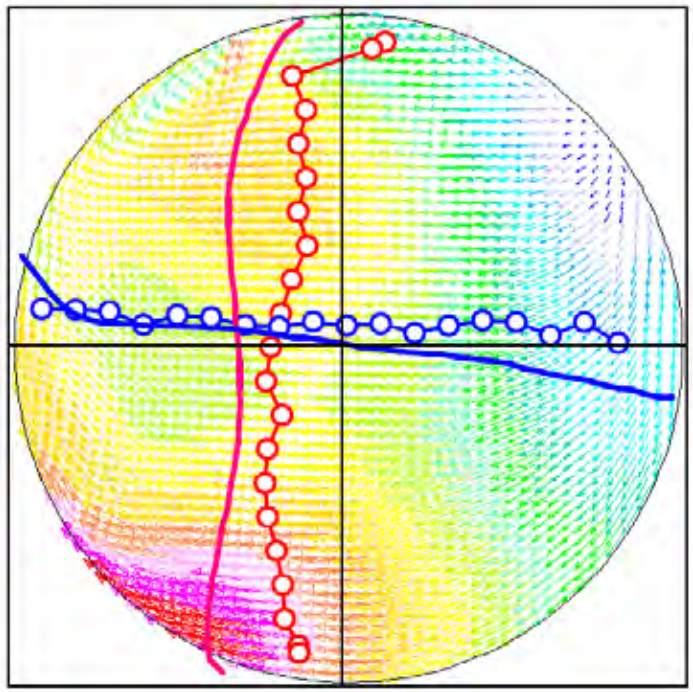

Z=-50 mm

Velocity magnitudes at X direction of the simulation is lager those of the experiment. The tendency of the velocity distributions are same with both conditions.

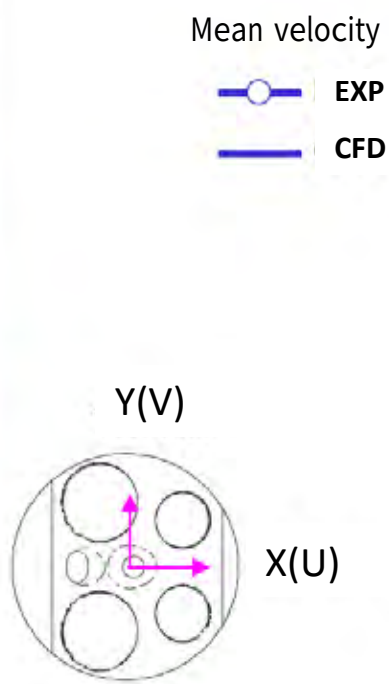

Swirl direction velocity distributions of transversal section at 240degree with TGV.

Result 3 Tumble ratio

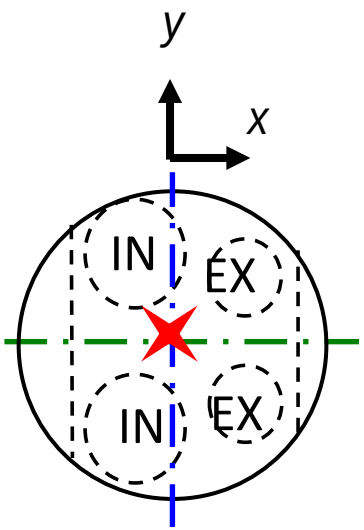

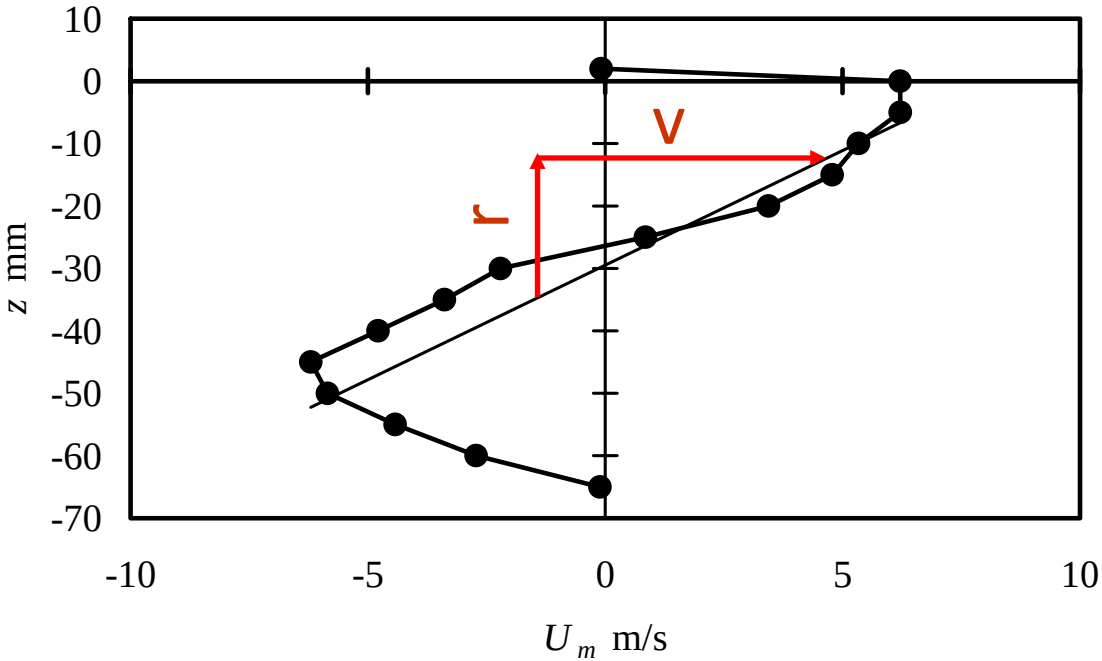

$$\text{Tumble ratio} = \frac{V}{r}$$

- Linear approximation by least squared method is obtained from velocity distribution in vertical section of the cylinder.

- It assumes that the angular velocity is inverse number of the gradient of that.

- This shows the simple tumble ratio in this presentation.

Tumble ratio

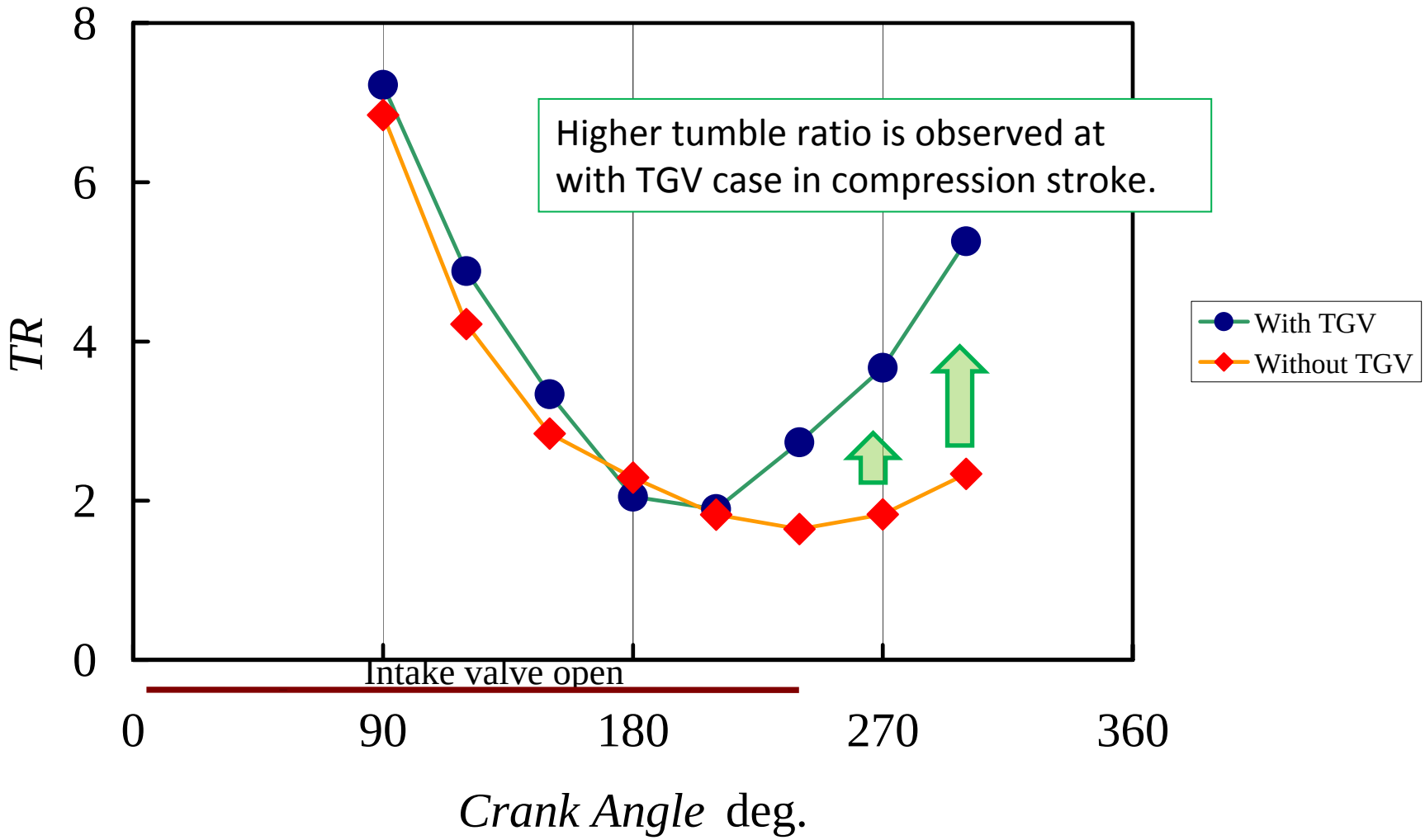

CONCLUSION

- Velocity distributions in two-directions are obtained with each crank angle. The database can be used for verification of CFD results.

- The difference in the flow near the inlet valve with and without the TGV is clearly shown. The flow directed to the wall becomes weak when the TGV exists.

- The effect of TGV is clarified by the experimental data. The effect of the TGV is remarkable in the upper side of the cylinder.

Thank you for your attention.

Turbulence Characteristics in the Cylinder of a 4-stroke Motored Engine by Means of LDA

* Tomio OBOKATA, Masaaki KATO and Tsuneaki ISHIMA

Department of Mechanical System Engineering, Gunma University
1-5-1 Tenjin, Kiryu, Gunma 376-8515, Japan

Makoto KANEKO

Fuji Heavy Industries Ltd.
3-9-6, Osawa, Mitaka-shi, Tokyo 181-8577, Japan

Key Words: Flow measurement, LDA/LDV, in Cylinder flow, Modeling

ABSTRACT

A series of experiment of the in-cylinder flow measurement has been carried out by using a laser Doppler anemometer (LDA). The purpose of the study is for making standard database of the flow structure of in-cylinder flow. The database can be used for the verification of the numerical simulation. The velocity components of vertical- and swirl-directions are measured individually. The test engine made by Fuji heavy industrial has transparent sapphire cylinder for optical access. The test condition is 600 rpm with motoring condition. The mean velocity maps are indicated by using ensemble averaged data with crank angle window of 1 degree. The rms velocity is also calculated from the data. The flow structure by each crank angle can be clarified. In addition, the effect of tumble generation valve (TGV) on the flow structure is also evaluated.

INTRODUCTION

The in-cylinder flow of the internal combustion engine is one of the basic physical phenomena. It is important for obtaining better thermal efficiency and less harmful exhaust gas of the internal combustion engine. The in-cylinder flow becomes important year by year because current technology of the internal combustion engine like as gasoline direct injection system requires optimum mixture which is formed by spray and in-cylinder flow. Hence, in order to improve the combustion process of the internal combustion engine, the flow characteristics of the in-cylinder flow has to be clarified. With this situation, there are many experimental research works about the in-cylinder flow [1-4]. Although the experimental works are performed successfully, there is no common understanding for gas flow due to intermittent, highly turbulent and 3-dimensional complex flow field in actual engine. Up to the recent years, the shapes of combustion chamber, piston head, and also intake port are mainly decided by trial and error. Therefore, the common understanding of for the in-cylinder flow is needed.

In this study area, numerical simulation is one of the important tools for obtaining the velocity characteristics. However, verification of the results of the numerical simulation has a lot of difficulties because of a lack of experimental data in good accuracy. The purpose of the present study is to prepare the standard database on the turbulent characteristics of in-cylinder flow velocity. The standard database is requested the data at wide area, 2- or 3-components velocity information. From this point of view, the previous works [1-4] were not enough and the measurement of new data set of in-cylinder flow is planed. The present data can be commonly used for some numerical research group of RC226 in JSME.

EXPERIMENTAL SETUP

2.1 Test Engine

Table 1 shows the specifications of test engine. The engine is 4-stroke and single cylinder type. The bore and stroke is 96.9 mm x 74 mm. The shapes of combustion chamber and piston head are pent roof and flat shape, respectively. The cylinder is made by sapphire which

Table 1 Engine specifications.

Engine type	4-stroke, Single cylinder
Combustion chamber	Pentroof type
Bore × Stroke	96.9 mm×74 mm
Displacement	545.7 cc
Compression ratio	11.5
Intake valve opening	4 deg.
Intake valve closure	240 deg.
Exhaust valve opening	485 deg.
Exhaust valve closure	5 deg.

Table 2 LDA properties.

Wave length	632.8 nm
Beam separation	50 mm
Beam diameter	1.35 mm
Focal length	300 mm
Full beam cross angle	9.52 °
Calibration factor	3.81 m/s/MHz
Diameter of waist	179 μm
Measuring volume length	2.26 mm
Measuring volume width	179 μm
Shift frequency	10 MHz

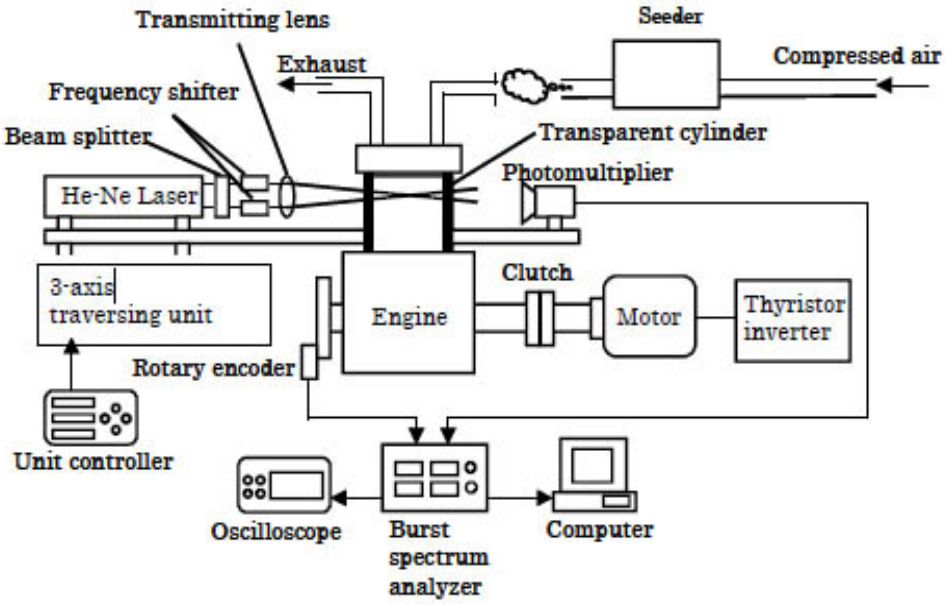

Fig. 1 Experimental setup.

makes ones for optical access. The measurement is tested under the motoring condition with 600 rpm of engine speed in the experiment. Since the present work is the first step of making standard database, the engine speed is decided as 600 rpm, which is reasonable to evaluate the idling operation of engine. The engine has tumble generation valve (TGV). The change in the velocity pattern with and without TGV is evaluated. Figure 1 shows the arrangement of experimental apparatus. The crank angle of the engine is monitored with a rotary encoder. All of the velocity information is analyzed by the ensemble averaged method in this report.

2.2 Measurement setup and methods

The measurement has been carried out by using a laser Doppler anemometer (LDA). The LDA consists of He-Ne laser (MELLES GRIOT 17mW) and burst spectrum analyzer (BSA, Dantec 57N20). Forward scattering mode is applied for better signal quality and data rate. Frequency shift which uses for measuring the negative velocity is 10 MHz. Table 2 shows detail property of the LDA. The origin of the coordinate system is on center of the piston head at TDC. The coordinate system is shown in Figure 2. The cylinder axis is *z*

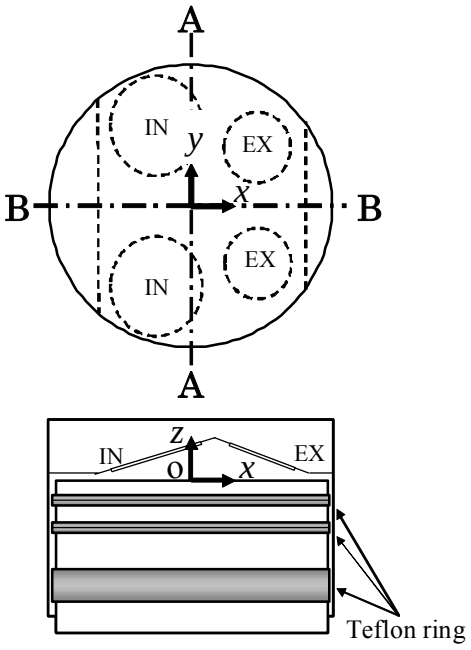

Fig. 2 Coordinate system.

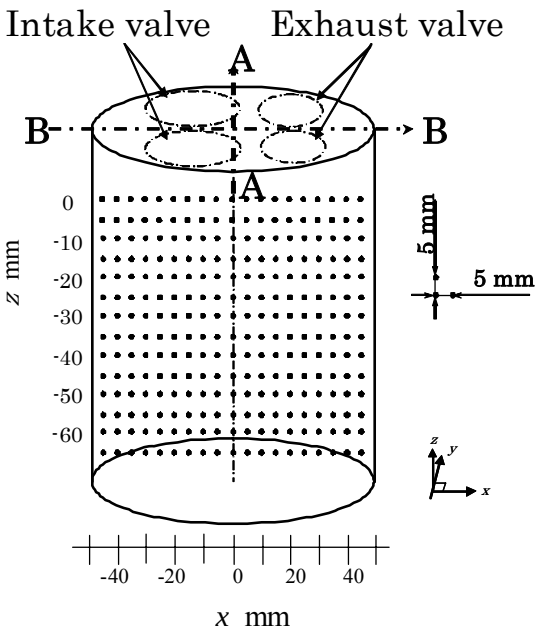

Fig. 3 Measuring positions.

direction. B-B plane is on center line between intake and exhaust valves and is set to *x*-*z* plane. A-A plane is perpendicular to the B-B section and is set to *y*-*z* plane.

The velocities of cylinder axis and swirl directions on the A-A and B-B planes are measured. The measurement positions are each 5 mm in - 45 mm ≤ *y* ≤ 45 mm and - 65 mm ≤ *z* ≤ 7 mm of A-A plane, and - 45 mm ≤ *x* ≤ 45 mm and – 65 mm ≤ *z* ≤ -10 mm of B-B plane. These positions are shown in Figure 3. In the experiment, the velocities from the intake valve are also measured. The measurement positions are at *x* = 10 mm, *y* = -30 mm and *z* = 9, 7, and 4mm and at *x* = -28 mm, *y* = -30 mm and *z* = 2, 0, and -2mm. 50000 samples are obtained at all of the measurement points. The instantaneous velocity components of *U*, *V* and *W* are directed to *x*, *y* and *z*, respectively. The mean velocity (U_m, V_m and W_m) and fluctuating intensity of instantaneous velocity (u_{rms}, v_{rms} and w_{rms}) are indicated by using the ensemble averaged data with crank angle window of 1 degree. The measurements are repeated several times and the accuracy and repeatability is checked.

Table 3 Tracer particles.

TiO_2 (KURONOS TITAN 2220)	
Mean particle size	0.4 μm
Density	4.0 g/cm^3
SiO_2 (Degussa AEROSIL R812)	
Mean particle size	7 nm
Density	2.2 g/cm^3

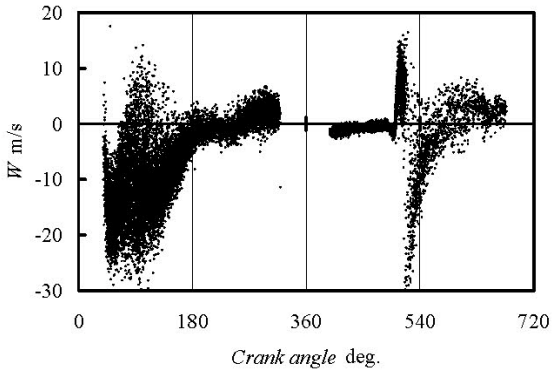

(a) Instantaneous velocities in many cycles with TGV

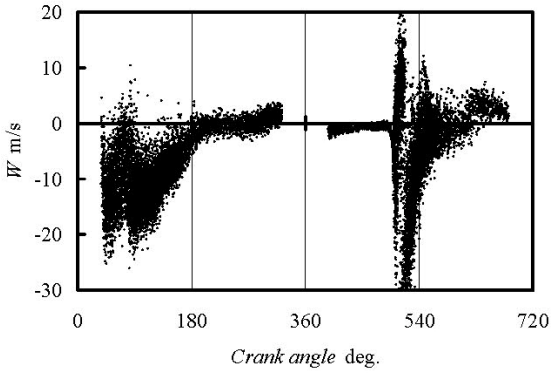

(b) Instantaneous velocities in many cycles without TGV

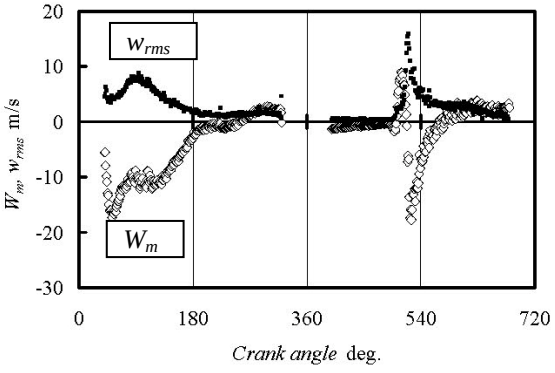

(c) Mean and fluctuating velocity with TGV

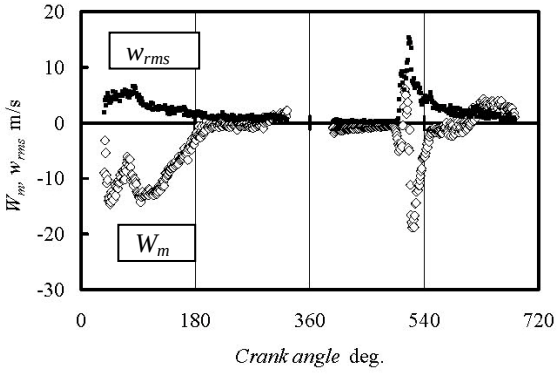

(d) Mean and fluctuating velocity without TGV

Fig. 4 Examples of axial velocity data measured by LDV with TGV or without TGV (Engine speed: 600 rpm, Motoring, WOT).

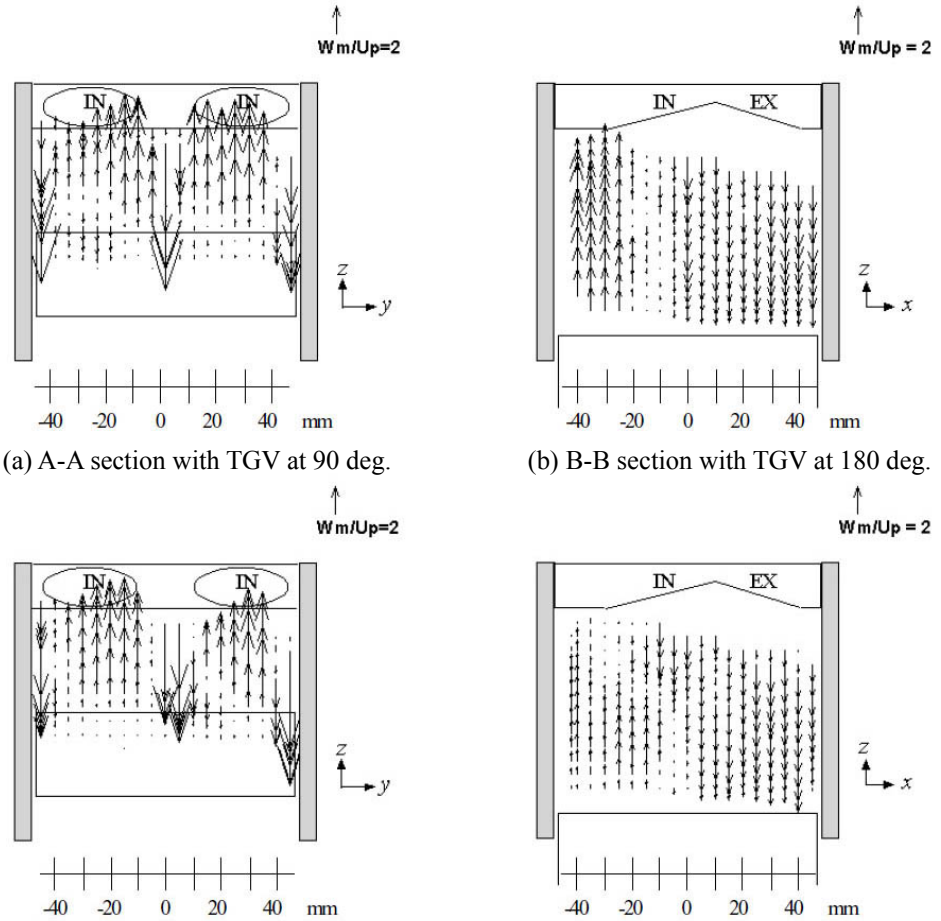

(a) A-A section with TGV at 90 deg. (b) B-B section with TGV at 180 deg.

(c) A-A section without TGV at 90 deg. (d) B-B section without TGV at 180 deg.

Fig. 5 Ensemble-averaged mean velocity distributions of W_m at vertical section (Engine speed: 600 rpm, Motoring, WOT, at CA = 90 deg. and 180 deg.).

The LDA measurement needs tracer particles. In the study, Titanium dioxide (TiO_2) of 0.4 μm in diameter is used for the tracer particle. For decrease in the effect of the humidity, Silicone dioxide (SiO_2) of 7 nm is added with 2 % of weight ratio as the hydrophobic particle. Properties of the particles are shown in Table 3.

RESULTS AND DISCUSSIONS

3.1 Velocities in tumble direction with and without TGV

Figure 4 shows the axial velocities measured at x, y, z = 0, 0, -10mm attached with TGV (a and c) or without TGV (b and d). Figures 4 (a) and 4 (b) show the instantaneous axial velocity of W obtained within 100 rotation cycles. There are no data durations in the results because the incident laser beams are blocked by piston or intake valves in the cylinder. At the intake stroke from 0 to 180 degree of crank angle, the tendency of the velocity of W is same with both conditions. The W at compression stroke also shows same tendency. The data is more scattered with the TGV condition at both of intake and compression strokes. Since the flow field may be far from the firing condition after the TDC of 360 degree of crank angle, these are not treated in the paper.

The ensemble averaged mean velocity of W_m and fluctuating intensity of w_{rms} are plotted at Figure 4 (c) and (d). At the intake stroke, higher W_m velocities in minus direction are observed in "with TGV" case comparing with "without TGV" experiment. The negative velocity with TGV is 20 % larger than that of the case without TGV around 50 degree of crank angle. The w_{rms} with TGV is also larger than that of without TGV case at the same crank angle.

Figure 5 shows velocity distributions of A-A and B-B sections at 90 and 180 degrees of crank angle. The figure indicated both flow fields of with and without TGV conditions. The velocities are normalized by the mean piston velocity of U_p = 1.48 m/s which corresponds to the engine speed of 600 rpm. From the comparison between Figs. 5 (a) and (c), it shows similar velocity distribution. It seems that the TGV has less effect on the velocity pattern in the plane. In detail, velocity magnitude with TGV is larger than that of without TGV case. Large velocity region can be observed at cylinder center line (y = 0 mm) and near the cylinder wall (y = ± 45 mm). There is reverse flow at the behind of intake valves.

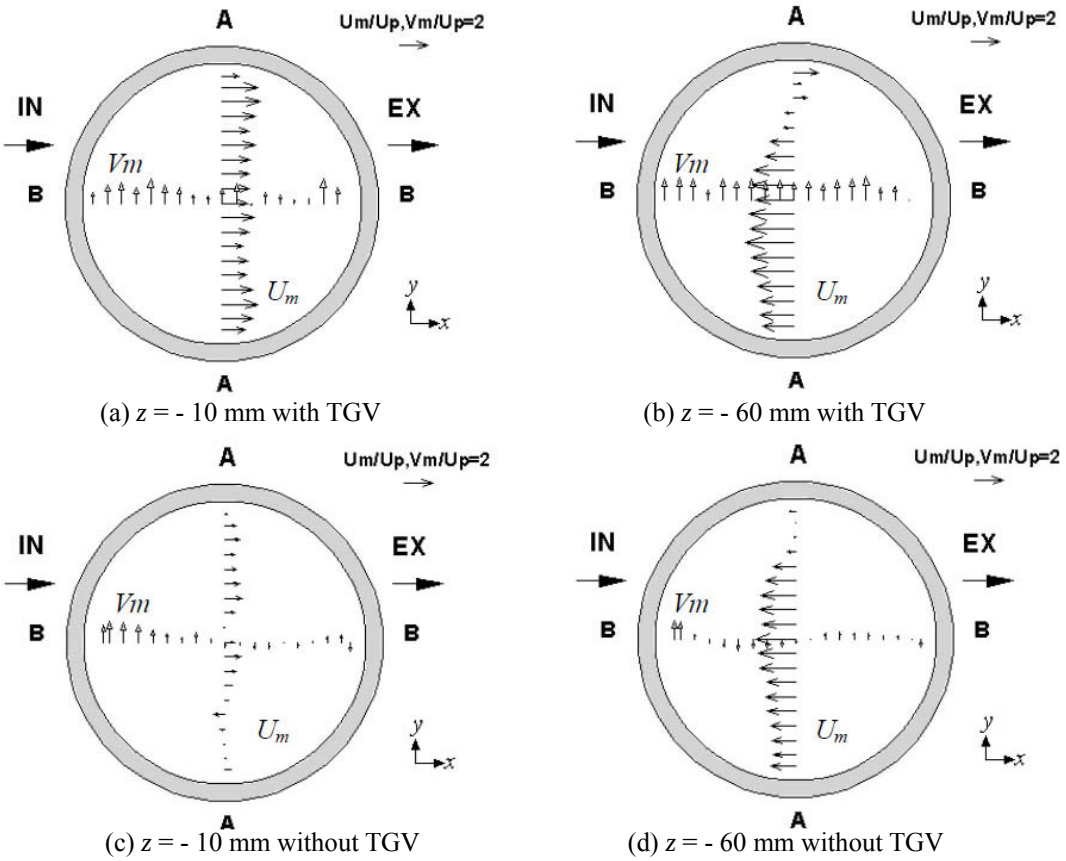

(a) z = - 10 mm with TGV (b) z = - 60 mm with TGV

(c) z = - 10 mm without TGV (d) z = - 60 mm without TGV

Fig. 6 Ensemble-averaged mean velocity distributions of U_m and V_m at transversal section (Engine speed: 600 rpm, Motoring, WOT, z = - 10, - 60 mm at CA = 180 deg.).

In the B-B section as shown in Figs. 5 (b) and (d), the TGV affects the velocities at intake valve side of B-B plane at 180 degree of crank angle. The results indicate the strong tumble motion with TGV condition. It seems that the flow with TGV has a biased velocity distribution on the intake valve. Since the velocity with TGV at the wall side of the intake valve seems weak due to the TGV, the upward flow is not disturbed by the flow from the intake valve. This point is explained detail after.

3.2 Velocities in swirl direction with and without TGV

Figure 6 shows velocity distributions of z = -10 and -60 mm planes at 180 degree of crank angle. The velocities are measured in only A-A and B-B planes. The mean velocities of U_m and V_m is normalized by mean piston speed of U_p = 1.48 m/s under engine speed of 600 rpm. It is shown from Figs. 6(a) and 6(b) that the U_m changes its direction by the measurement z planes. The V_m is not changed direction and velocity magnitude drastically. In addition, the magnitude of V_m is smaller than that of U_m. The results indicate the tumble motion is important and there is very small swirl motion in the present engine. Comparing with the existence of TGV, it is shown that the velocity at z = - 10 mm in x direction changes in its magnitude. When the TGV exists, the velocity U_m in x direction becomes larger than that of without TGV condition. On the other hand, velocity V_m in y direction has small changes with conditions. At z = - 60mm as shown in Figs. 6 (b) and (d), the velocity distributions are nearly equal to each other. The effect of the TGV seems to become small compared with upper side of the cylinder.

Combination on the velocity distributions in A-A plane at z = - 10 and - 60 mm provides the tumble motion. The results indicate that the TGV creates strong tumble motion. On the other hand, the TGV has less effect on the swirl motion.

3.3 Flow velocity near the intake valve

Figure 7 shows the velocity vectors around the intake valve. The vectors are obtained at 60, 90 and 120 degree of crank angle. At 60 degree of crank angle, the right hand side which is cylinder center side with TGV is slightly larger than that of the case without TGV. The difference in the velocity pattern at the crank angle is not clear. At 90 degree of the crank angle, the velocity at the right hand side with TGV becomes larger than that of without TGV case. The velocity at the left hand side which is directed to the wall becomes weak when the TGV exists. The difference in the left hand side is more remarkable than that of the right hand side. At the 120 degree of

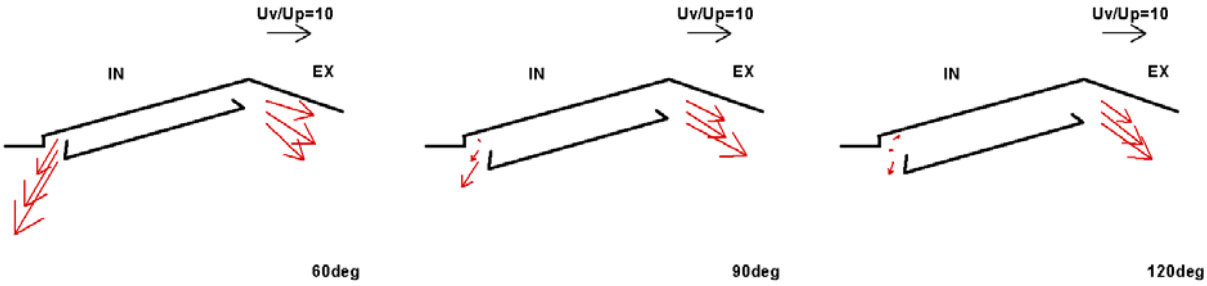

(a) with TGV

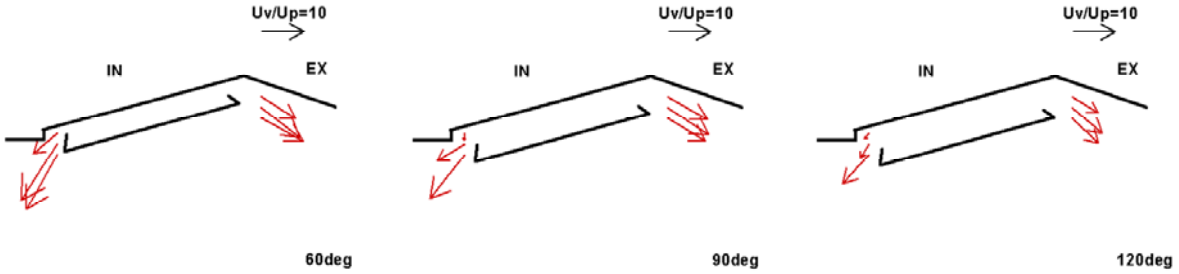

(b) without TGV

Fig. 7 Flow velocity through a intake valve.
(Engine speed: 600 rpm, Motoring, WOT, at CA = 60, 90 and 120 deg.).

the crank angle, the velocity tendencies are almost same with that of the 90 degree of crank angle.

The strong flow directed to the wall disturbs the upward flow near the wall. The effect of the flow can be appeared in the upper side of the cylinder. The results of Fig. 7 are one of the evidences of the consideration of tumble motion described above.

CONCLUSIONS

LDA measurements are performed in order to construct the database for verification of numerical simulation. The effect of the tumble generation valve (TGV) is evaluated by velocity distributions. The concluding remarks are follows:

1. Velocity distributions in two-directions are obtained with each crank angle. The database can be used for verification of numerical simulations.
2. The effect of TGV is clarified by the experimental data. The effect of the TGV is remarkable in the upper side of the cylinder.
3. The difference in the flow near the inlet valve with and without the TGV is clearly shown. The flow directed to the wall becomes weak when the TGV exists.

Acknowledgements

The authors would like to thank to all students who related with the experiments and analysis.

REFERENCES

[1] UEKI, H., ISHIDA, M. and EGAMI, H., Study on In-Cylinder Flow of Direct Injection Diesel Engine by LDV Measurements, Transactions of JSME, Series B, Vol.55 No.511(1989), pp.910-915 (in Japanese)

[2] OBOKATA, T., HANADA, N., KUWAHARA, H. and KURABAYASHI, T., Measurement of Gas Velocity in a Combustion Chamber of a Small-Size, two-Stroke S.I. Engine by LDA, Transactions of JSME, Series B, Vol.54 No.505(1988), pp2687-2693 (in Japanese)

[3] KANEKO, M., IKEDA, Y. and NAKAJIMA, T., Tumble Generator Valve (TGV) Control of In-cylinder Bulk Flow and Its Turbulence Near Spark Plug in SI Engine, SAE Paper, No.2001-01-1306 (2001)

[4] MORIYOSHI, Y., KAMIMOTO, T. and YAGITA, M., Prediction of Cycle-to-Cycle Variation of In-cylinder Flow in a Motored Engine, SAE Paper No. 930066.

1.4G High Compression Ratio Operation of SI Engines without Knocking by Controlling Piston Speed Near TDC

*Yasuo Moriyoshi

Department of Mechanical Engineering, Chiba University
1-33 Yayoi-cho, Chiba 263-8522, Japan

Koji Morikawa, Makoto Kaneko and Hiroshi Oiwa

FujiHeavy Industries
3-9-6 Osawa, Mitaka,Tokyo 181-8577, Japan

Key Words: Gasoline Engine, Thermal Efficiency, Knocking, High Compression Ratio, Cranking Mechanism

ABSTRACT

A new gasoline combustion engine system with high compression ratio was studied and proposed in order to achieve higher thermal efficiency than that of a conventional SI engine. A special cranking mechanism was adopted which allowed the piston to move rapidly near TDC. Some mechanisms were proposed and two of them were designed and built for the testing. The experimental results showed that knocking was avoided and better indicated thermal efficiency was obtained. An inconstant speed gear mechanism with compression ratio of 14 could be operated up to 3000 r/min and thermal efficiency was improved by 18% compared to a conventional engine with compression ration of 10. Also, a cam mechanism driven by a planetary gear was tested to achieve higher engine speed up to 4000 r/min, but the improvement of thermal efficiency was not so large as much as of the inconstant speed gear mechanism.

INTRODUCTION

Various methods have been tried in order to improve thermal efficiency of a gasoline engine, such as to enhance theoretical thermal efficiency by increasing compression ratio, to induce lean burn and to improve mechanical efficiency by lowering the friction loss for prime methods. However, no method to achieve high brake thermal efficiency as much as of a diesel engine has been put into practical use. For substantial improvement of thermal efficiency, the ways to realize a low-cost gasoline engine that can be operated with high compression ratio have been sought. The major obstacle for the development is the knocking phenomenon. Although many research works have been conducted to suppress knocking in the aspect of combustion and fuel, the fundamental solution is not found yet [1-6]. The authors, therefore, focused on suppressing knocking in the aspect of the cranking mechanism with high compression ratio for higher thermal efficiency. Some results including numerical simulations, actual engine tests and combustion analysis have been achieved and published by the authors [7-9].

In this paper, methods how to achieve a rapid piston motion near TDC even for high engine speed are discussed first. Then, experimental performance test results for two test engines are indicated. As a result, some useful items to realize this unique idea into production were deduced.

SUPPRESSION OF KNOCKING

Piston Speed Control Mechanism

In order to make a rapid piston movement near TDC, three methods were examined; i) inconstant speed gear mechanism, ii) planetary eccentric cam mechanism and iii) link mechanism. The schema of each method is indicated in Fig. 1 while the specifications are listed in Table 1.

Inconstant speed gear mechanism enables the rapid piston movement near TDC by inserting a pair of special shaped gears between the power output shaft and the crank shaft. Three types of gears; elliptic, leaf-shape and modified leaf-shape with off-set gear center shown in Fig. 2 were examined.

A planetary eccentric cam mechanism is to put an eccentric cam at the junction between the big-end of connecting rod and the crank pin. Because this cam makes a rotational motion by the motion difference between the internal gear along the periphery of the crank and the external gear along the periphery of the cam, the piston speed is determined by the variations of the eccentric amount and the phase. That is, the piston motion depends on the eccentric amount and the reduction ratio. In this study, the reduction ratio and the eccentric amount were set at 3 and 5.26, respectively.

The link mechanism is to increase the piston speed near TDC. Two kinds of systems were examined; one is with a modulation crank and the other is using a slider. Parameters in each method were optimized.

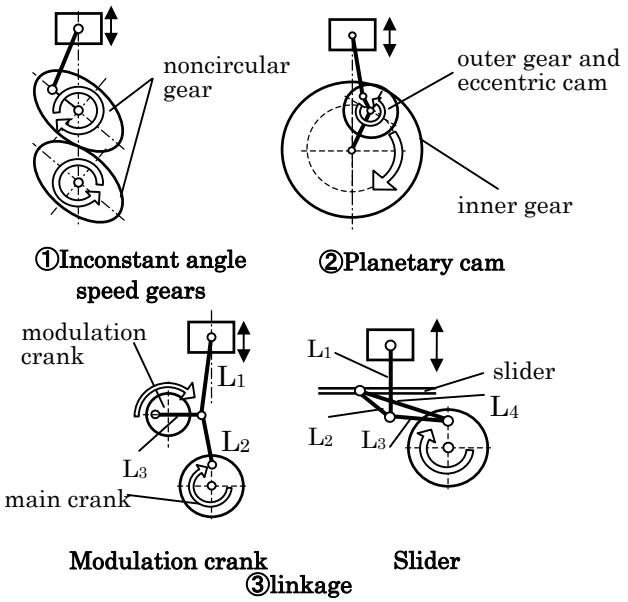

Fig. 1 Rapid piston moving systems near TDC

Table 1 Engine specifications of rapid piston moving systems

Specifications of combustion region	
Bore x Stroke	ϕ 99.5 x 79 mm
Connecting rod	185 mm
Displacement	614 cm^3
Compression ratio	10 ~ 14
Ratio of specific heat	1.23 - 1.40 (function of temperature)
Inconstant angle speed gears	
Crank angler speed	0.5-2.0 times as base sys.
Planetary cam	
Gear ratio of planetary gear	3
Cam eccentricity	5.26 mm
Modulation crank	
Proportion of rod length	L1 : L2 : L3 = 5 : 2 : 3
Slider linkage	
Proportion of rod length	L1 : L2 : L3 : L4 = 5 : 2 : 1 : 6

Figures 3 and 4 show the piston position and the velocity with power shaft angle, respectively. Each mechanism shows a rapid piston motion near TDC. The fastest one is of elliptic, next in the order, modulation crank, leaf-shape and modified leaf-shape.

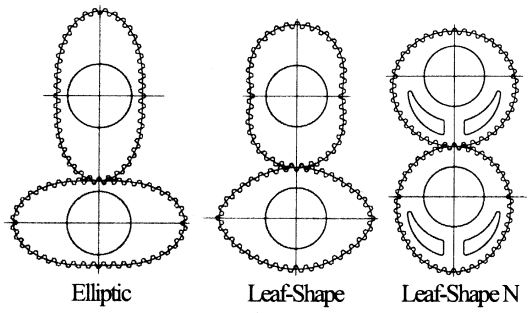

Fig. 2 Gear systems

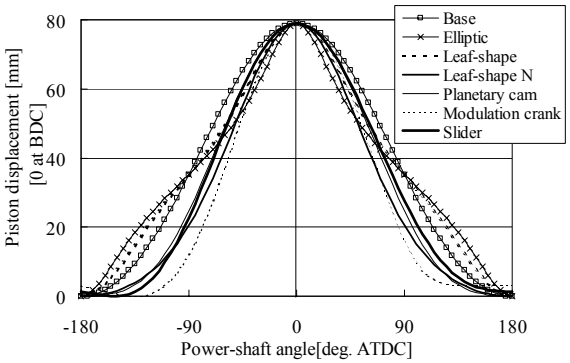

Fig. 3 Piston displacement vs. power-shaft angle

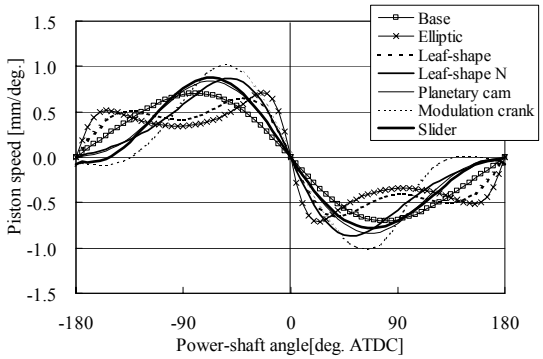

Fig. 4 Piston speed vs. power-shaft angle

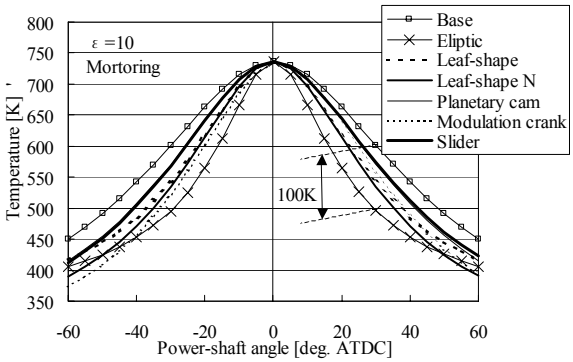

Fig. 5 In-cylinder temperature vs. power-shaft angle

Figure 5 indicates adiabatic gas temperature without firing at compression ratio of 10. At 30 deg. ATDC, corresponding to the combustion final phase, the gas temperature of elliptic is 100 K lower than of conventional mechanism. This must give a large effect on knocking occurrence.

Optimization by Numerical Simulation

A numerical simulation was performed in order to quantify the suppression of knocking and improvement of thermal efficiency. It was performed in the aspect of suppression of knocking and heat loss reduction in order to optimize them. The Woschini formula [10] and integration values of Livengood-Wu [11] (hereafter referred to as L-W) were respectively applied in order to calculate the heat loss and a prediction of knocking occurrence. Details of the calculation method can be found in the authors' references [7-8].

Predictions of thermal efficiency at engine speed of 600 r/min and 2000 r/min are indicated in Figs. 6 and 7, respectively. Compression ratio is 14, ignition timing MBT (Minimum advance for Best Torque), equivalence ratio 1, volumetric efficiency 100%. Compared to the conventional system, the result indicates that thermal efficiency is improved in most cases at 600 r/min while it is improved in the cases with short combustion period at 2000 r/min. The effect is remarkable in the order, elliptic, leaf-shape N, modulation crank and leaf-shape, corresponding to the piston speed rapidness. Here, it should be noted that as the combustion period increases, thermal efficiency deteriorates due to the decrease in degree of constant volume.

Next, the tolerance to knocking was estimated. A knocking index of L-W integral was calculated for 600 and 2000 r/min conditions as shown in Figs. 8 and 9, respectively. The calculated L-W values are normalized using the value at the condition of base engine with compression ratio 10, volumetric efficiency 100%, ignition at 3 deg. BTDC, combustion period 20 deg., and engine speed 2000 r/min. In both Figs., combustion period and ignition timing were set at 40 deg. and TDC, respectively. The tendency is the same for two engine speeds. The tolerance to knocking is larger in the order, elliptic, leaf-shape and leaf-shape N. Thereby, the gear mechanism was found advantageous to avoid knocking.

EXPERIMENTAL APPARATUS

Leaf-shape Gear Engine

The specifications for the single-cylinder engine are shown in Table 1. The engine has a typical port fuel injection system. Tests were performed using the regular gasoline and with compression ratio of 10, 12 and 14.

Figure 10 shows the outline of the experimental apparatus. Each gear system was installed in a gearbox on the output end of the crankshaft for changing crank angle speed. The output side of the gearbox is connected to a dynamometer, which controls the apparatus operation. The camshaft is driven by the output shaft of the gearbox in order to keep its angle speed constant. With these systems, the output shaft runs at constant angular velocity while the crankshaft runs at inconstant angular velocity.

Planetary Eccentric Cam Engine

The maximum engine speed of the above mentioned gear mechanism was limited up to 3000 r/min because of heavy vibrations. This vibration was caused by the reaction force of torque fluctuation in one rotation. One of the countermeasures for this vibration is to equip a balancer shaft of torque balance.

On the other hand the authors have devised a new compact mechanism to achieve a rapid piston movement near TDC. This mechanism works without inconstant speed of crankshaft. A cam was fixed in the crankshaft pin together with a con-rod big end. The cam is rotated by a planetary gear system The planetary gear system does not transfer an engine torque despite the gear mechanism of the elliptic and the leaf-shape gear systems transfer an engine torque. A strength of the gear of new mechanism is not an issue. A new engine with the new mechanism is shown in Fig.11. Table 3 shows the engine specifications.

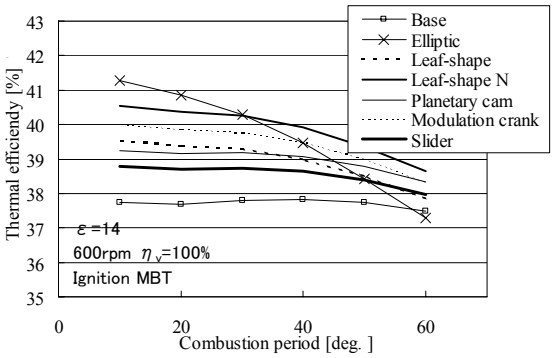

Fig. 6 Calculated thermal efficiency vs. combustion period

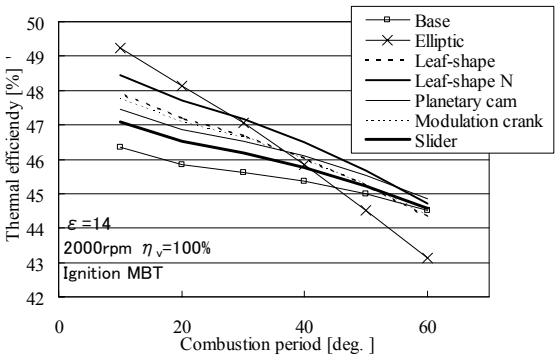

Fig. 7 Calculated thermal efficiency vs. combustion period

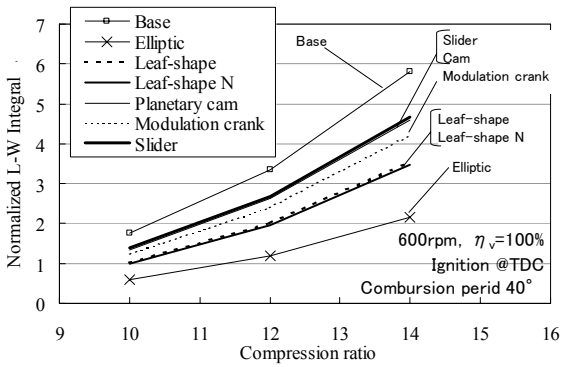

Fig. 8 Normalized L-W integral vs. compression ratio

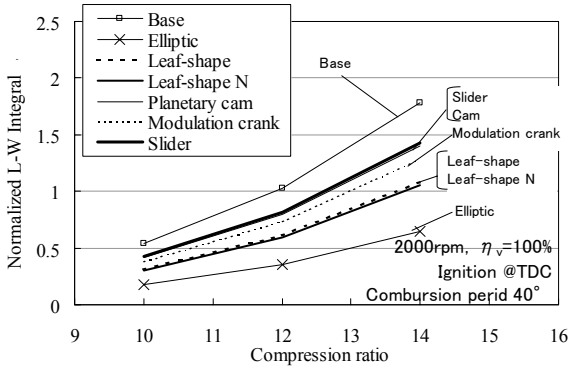

Fig. 9 Normalized L-W integral vs. compression ratio

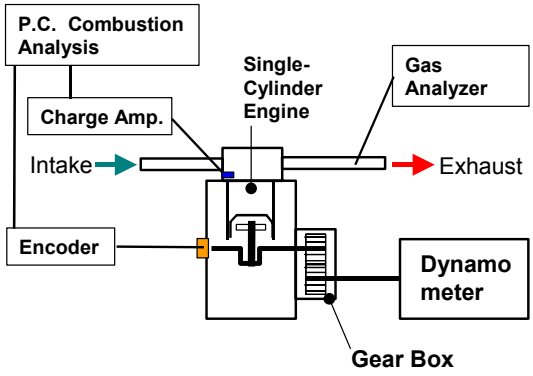

Fig.10 Experimental apparatus for inconstant speed gear mechanism

The relation between the piston displacement and eccentric amount is indicated in Fig. 12, while each locus of the big-end and the crank-pin is shown in Fig.13. As the eccentric amount increases, the piston speed increases, but BDC does not corresponds at +/-180 deg. when the eccentric amount exceeds a threshold. As a result, the eccentric amount was set at 4 mm.

Table 3 Specifications of planetary eccentric cam engine

Engine type	4-stroke single cylinder
Bore × Stroke	Φ75 × 60 mm
Connecting rod	113.4 mm
Fuel supply	Port injection
Displacement	265 cm^3
Compression ratio	14
Gear ratio of planetary gear	3
Cam eccentricity	4 mm

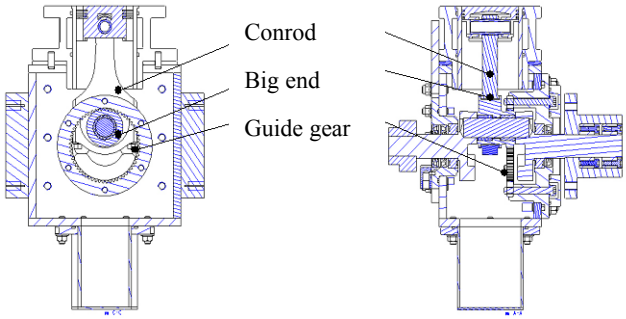

Fig.11 Planetary eccentric cam mechanism

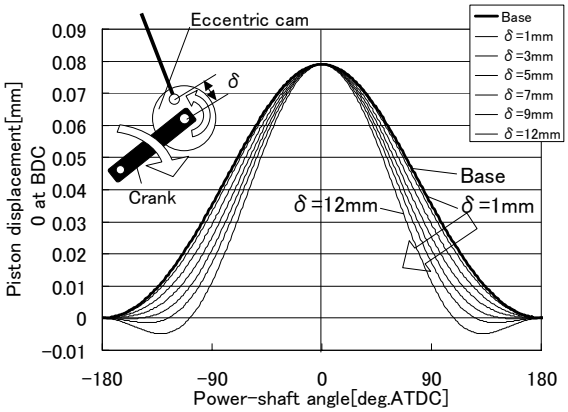

Fig.12 Piston displacement vs. power-shaft angle

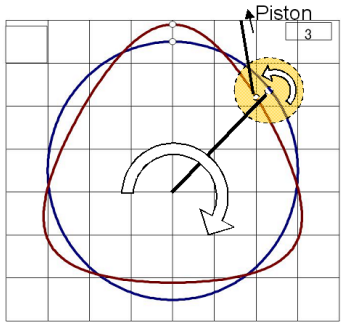

Fig.13 Locus of big-end and crank-pin with eccentric cam

TEST RESULTS AND DISCUSSION

Characteristics for Knocking Suppression

The characteristics of knocking suppression were investigated in extremely low engine speed range where knocking is prone to occur and also in a regular speed. At first, the base and leaf-shape system under the conditions of engine speed at 600 r/min, 80% load, equivalent ratio of 1, and compression ratio of 12. Because the base system was unable to run on regular gasoline due to excessive knocking, high-octane gasoline (RON=100) was used and could run at MBT in order to compare its effect to that of inconstant speed crank system.

In case of the leaf-shape system, the ignition timing could not be advanced to MBT, but the engine could run on regular gasoline when the ignition timing was retarded, which demonstrated the effects from accelerated piston speed near top dead center. However, the knocking could not be completely suppressed in case of the leaf-shape system and the fuel consumption was not as good as that of the base system due to longer combustion period. Thereby, a TGV (Tumble Generating Valve) was attached to the leaf-shape system in order to generate turbulence and facilitate quick combustion. This not only reduced required ignition advance angle but also allowed ignition at MBT, resulting in fuel economy improvement

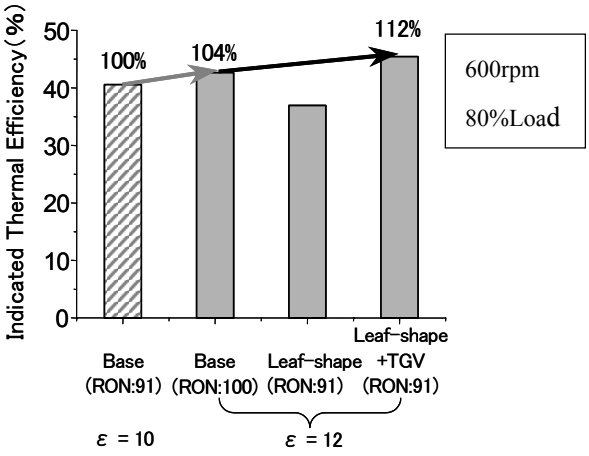

Fig.14 Comparison of indicated thermal efficiency

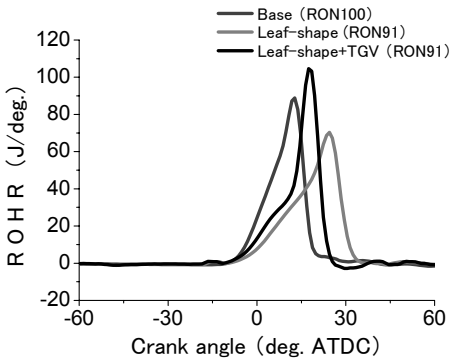

Fig.15 Rate of heat release of three engines (600 r/min)

Results at 600 r/min with Compression Ratio 12

Figure 14 shows a comparison of indicated thermal efficiency. The indicated thermal efficiency of the base system with the compression ratio of 10 is also shown here for comparison. The leaf-shape system with the TGV showed an improvement in fuel economy from the base system, approximately 8% and 12% at the compression ratio of 12 and 10 respectively. Figure 15 indicates rate of heat release. In the case of leaf-shape system, the ignition timing was retarded from the target in order to suppress knocking and its heat release and combustion speed was slower compared to the base system. In case of the leaf-shape system with the TGV, on the other hand, combustion speed was recovered and rapid combustion was attained especially in the last half, indicating a highly knocking-suppressive combustion pattern.

Operation with Compression Ratio of 14 at 2500 r/min

Tests at higher compression ratio of 14 and engine speed at 1600 and 2500 r/min were achieved. Figures 16 and 17 show thermal efficiency at 1600 and 2500 r/min, respectively. Values in the figure indicate the improved thermal efficiency rate compared to the base engine. At a condition of 1600 r/min and IMEP 800 kPa, the maximum improvement of 18.4% was attained. Much improvement was found at higher IMEP, especially for 1600 r/min conditions. For this reason, the decrease in heat loss was found as the combustion period indicated in Figs. 18 and 19 is shorter in higher IMEP. At higher engine speed, the improvement was worse because the decrease in heat loss becomes less due to longer combustion period. Regarding the relationship between the engine speed and improvement rate, higher engine speed conditions do not indicate high improvement rate as much as lower engine speed because the heat loss relatively decreases as engine speed increases.

Test Results of Planetary Cam Engine

The authors confirmed this engine can be operated with an engine speed from idling to 4000 r/min firing condition. The engine runs in WOT at MBT without knock at 600 r/min as indicated in Fig. 20. However, increasing the engine speed, knock occurred due to an increase in the combustion period as a TGV is not installed. Some method to enhance combustion must be installed to improve thermal efficiency.

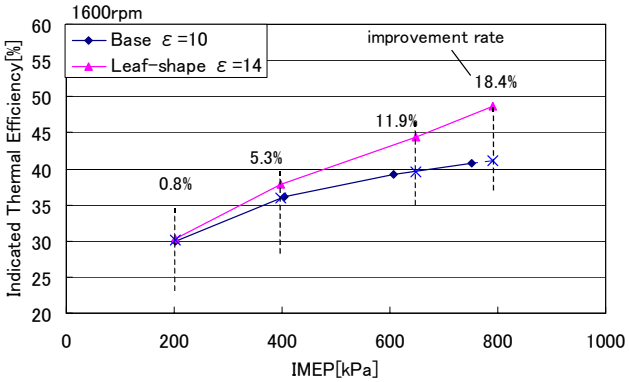

Fig.16 Indicated thermal efficiency vs. IMEP at 1600 r/min

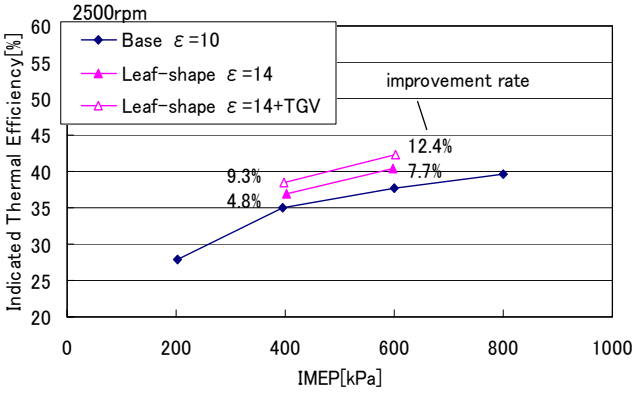

Fig.17 Indicated thermal efficiency vs. IMEP at 2500 r/min

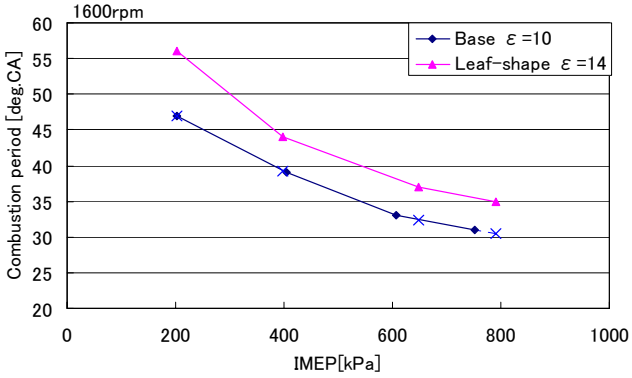

Fig.18 Combustion period vs. IMEP at 1600 r/min

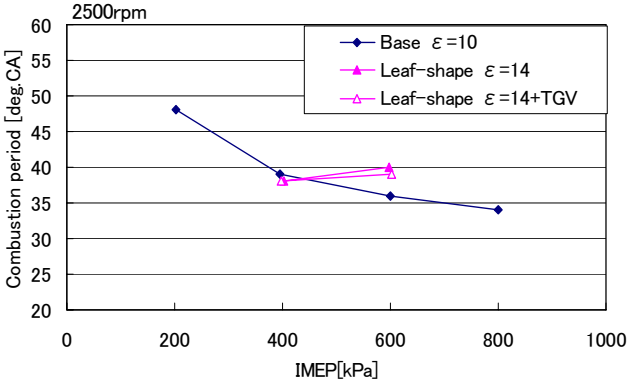

Fig.19 Combustion period vs. IMEP at 2500 r/min

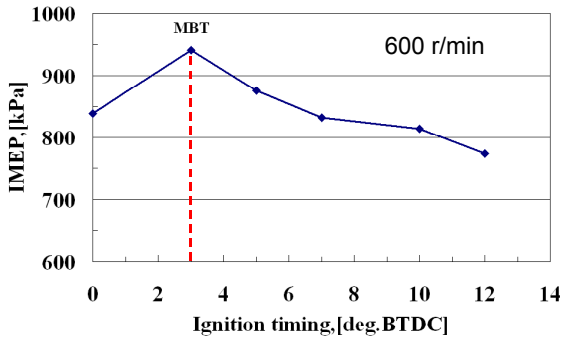

Fig.20 Ignition timing vs. IMEP of planetary cam system

CONCLUSIONS

(1) In order to avoid knocking and to improve thermal efficiency, the piston motion near TDC was made quick. To realize this, three kinds of mechanism, such as inconstant angle speed gears, a planetary cam and linkage systems were examined. Theoretically, the inconstant angle speed gears have the highest potential, but also have a vibration issue. Thereby, two kinds of mechanism of the inconstant angle speed gears and the planetary cam were designed and built for performance tests.

(2) The inconstant crank angle speed system with compression ratio 12 at 600 r/min showed approximately 12% improvement compared to the base engine (compression ratio 10) in the indicated thermal efficiency. When this engine was operated at 1600 r/min with compression ratio 14, 18% improvement was attained. Not only the increase in compression ratio but also the decrease in heat loss caused such high improvement of thermal efficiency.

(3) A planetary cam system with compression ratio 14 for higher engine speed was introduced and operated up to 4000 r/min. No knocking was confirmed at 600 r/min WOT and MBT operation. However, operations in higher speed caused knocking as the combustion period became long. Some method to enhance combustion speed must be installed.

Acknowledgements

This study was funded by NEDO (New Energy and Industrial Technology Development Organization).

REFERENCES

(1) J. Pan, C.G.W. Sheppard, A.Tindall,M. Berzins, S.V. Pennington and J.M. Ware, End Gas Inhomogeneity, Autoignition and Knock, SAE Paper No.982616

(2) Rudolf R. Maly, Rupert Klein, Norbert Peters, Gerhard Konig, Theoretical and Experimental Investigation of Knock Induced Surface, SAE Paper No.900025

(3) G. Konig and R. R. Maly, D.Bradley, A. K. C. Lau and C. G. W. Sheppard, Role of Exothermic Centres on Knock Initiation and Knock Damage, SAE Paper No.902136

(4) G. Konig, C. G. W. Sheppard, End Gas Autoignition and Knock in a Spark Ignition Engine, SAE Paper No.902135

(5) J. Pan and C. G. W. Sheppard, A Theoretical and Experimental Study of the Modes of End Gas Autoignition Leading to Knock in S. I. Engines, SAE Paper No.942060

(6) Hisato Hirooka, Sachio Mori and Rio Shimizu, Effects of High Turbulence Flow on Knock Characteristics, SAE Paper No.2004-01-0977

(7) K. Morikawa, M. Kaneko, Y. Moriyoshi and M. Sano, A Study on New Combustion Method of High Compression Ratio Spark Ignition Engine, SAE Paer No. 2005-01-0240

(8) Y. Moriyoshi, M. Sano, K. Morikawa and M.Kaneko, Drastic Improvement of Thermal Efficiency By Rapid Piston-Movement Near TDC, Int. J. of Automotive Technology, 7-3 (2006) 295.

(9) K. Morikawa, K. Makoto, Y. Moriyoshi, A New Gasoline Combustion System with High Thermal Efficiency by Rapid Piston-Movement Near TDC, Trans. of FISITA, No. F2006P168T (2006)

(10) G.Woschni, A Universally Applicable Equation for the Instantaneous Heat Transfer Coefficient in the Internal Combustion Engine, SAE Paper No. 670931

(11) Livengood, J. C. & Wu, P. C. 5th Symposium on Combustion (1955). 347

30th IEA-TLM 1.4G Spark-Ignition Engine, Capri (September 14-18, 2008)

Fuel and CO_2 concentration measurement near a spark plug in a spark ignition engine

Okayama University

Nobuyuki KAWAHARA
Eiji TOMITA

Key feature of fuel concentration near spark plug

-Cycle-by-cycle fluctuation
-Fuel concentration at spark timing
-Fuel distribution inside cylinder
-Residual gas concentration
.....

Mixture
(fuel, air, residual gas?)

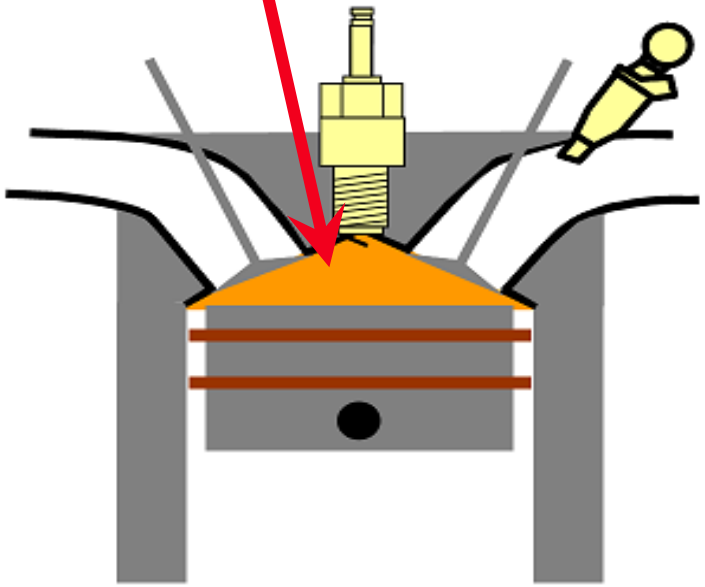

Measurement method

-Gas sampling
-LIF
-Raman scattering
-In situ infrared absorption

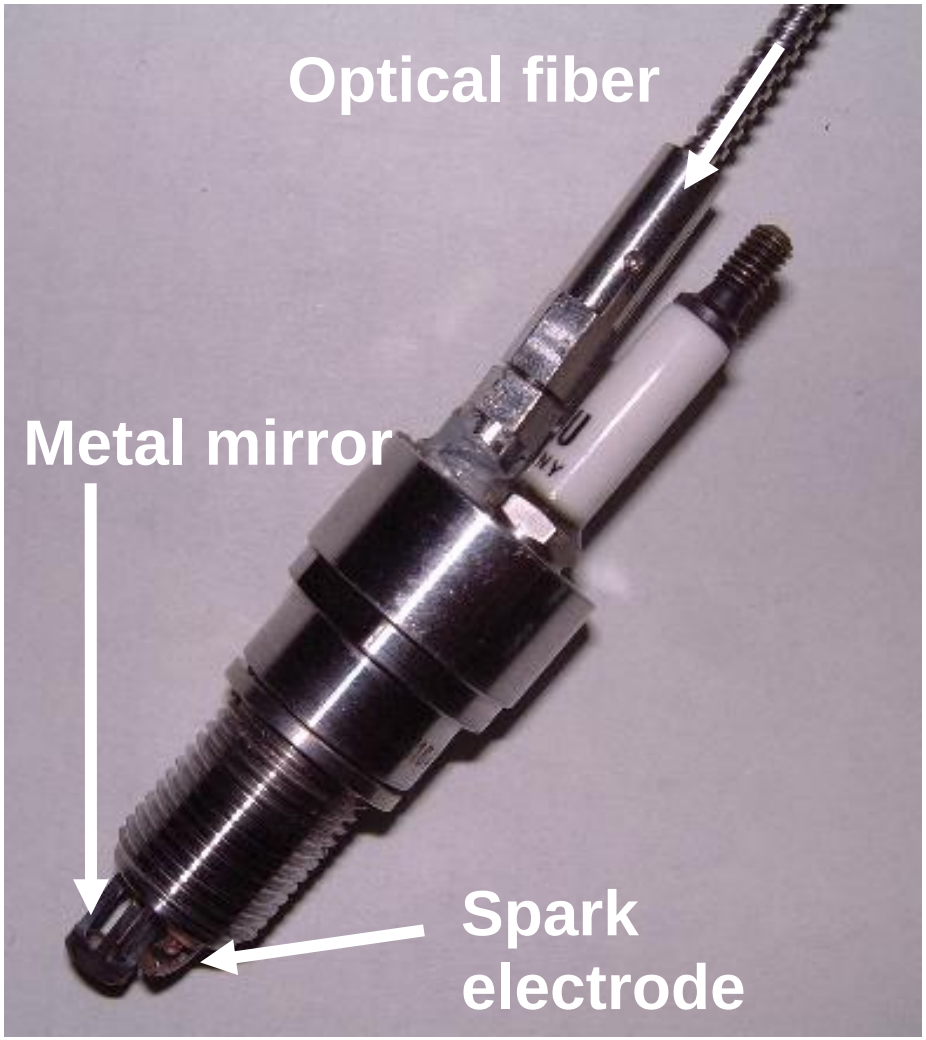

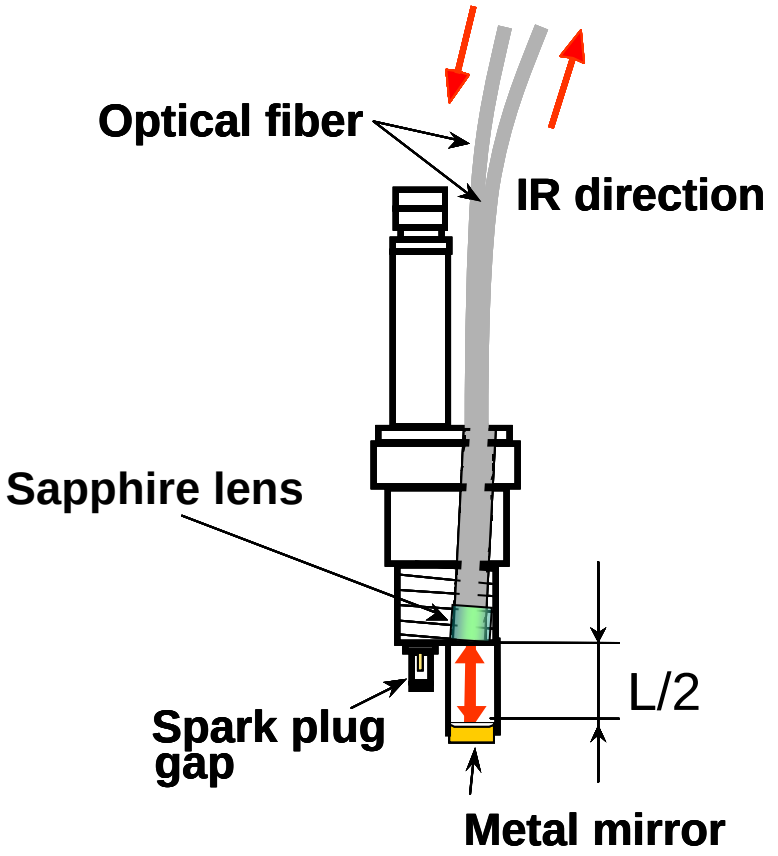

Schematic diagram of sensor

Sensor plug

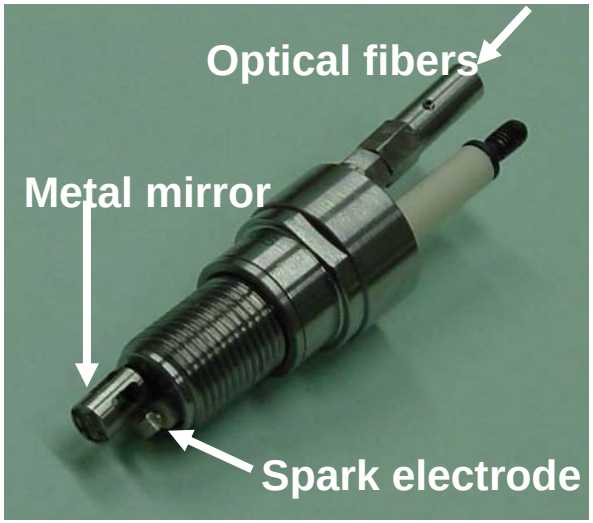

Data recorder

processor

Optical Fiber

Band Pass Filter

IR Detector for 3.39μm

He-Ne laser λ=3.39 μm

Collimator

In.

Ex.

Injector

Spark plug

IR sensor

Vibration isolator

IR Sensor system

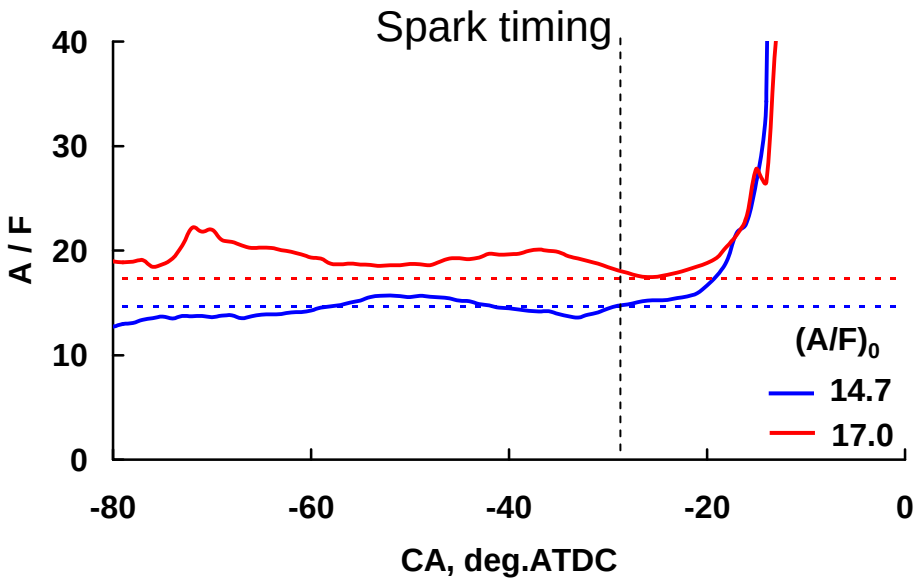

(a)θ_{inj}=-30deg.ATDC

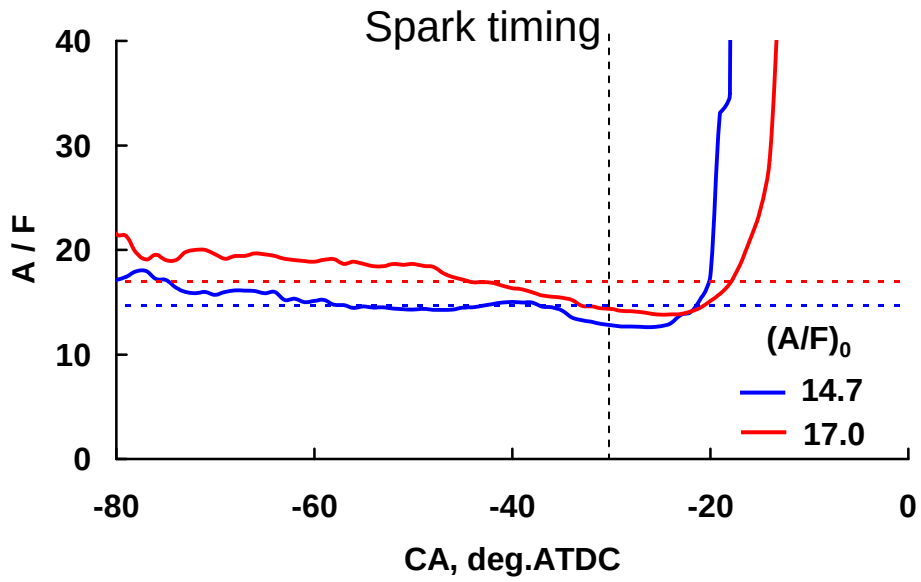

(b)θ_{inj}=120deg.ATDC

- Time-series of fuel concentration near spark plug
- Fuel concentration at the spark timing

Mixture preparation

	Gas sampling	Raman scattering	In-situ absorption method
Intrusive?	Intrusive ×	Nonintrusive□	Nonintrusive○
Spatial resolution	□	□	○
Window	w/o window□ applicable to actual engine	with window ×	w/o window□ applicable to actual engine
Response	ms □	ns□	μs○
Accuracy	□	□	○

Comparison of concentration measurement method

Purpose

- Selection of absorption lines of CO_2
  (HITRAN database)
- Absorption characteristics of CO_2
  (Effect of ambient pressure and temperature)
  (constant volume vessel)
- Developed system with spark plug sensor
  applied to a compression-expansion machine
  and to a port-injected SI engine

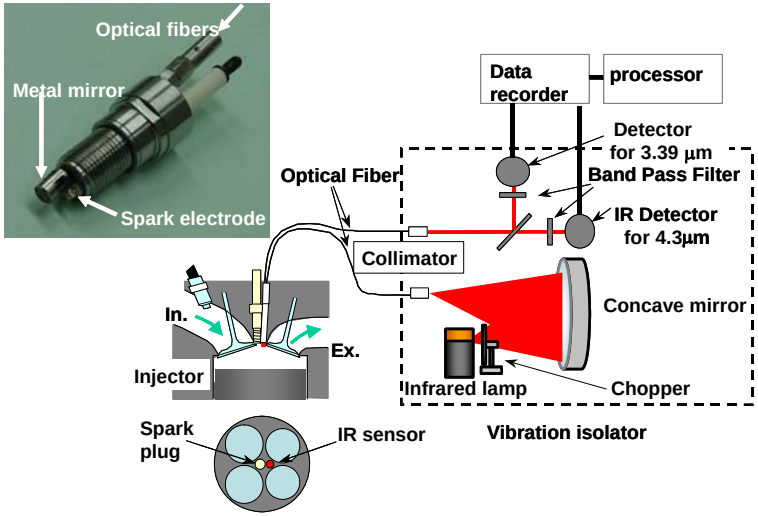

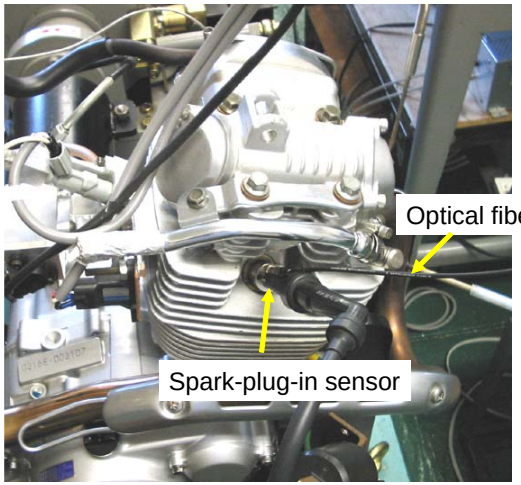

Purpose of Carbon Dioxide Measurement

- Selection of absorption lines of CO_2
  (HITRAN database)

- Absorption characteristics of CO_2
  (Effect of ambient pressure and temperature)
  (constant volume vessel)

- Developed system with spark plug sensor
  applied to a compression-expansion machine
  and to a port-injected SI engine

Contents

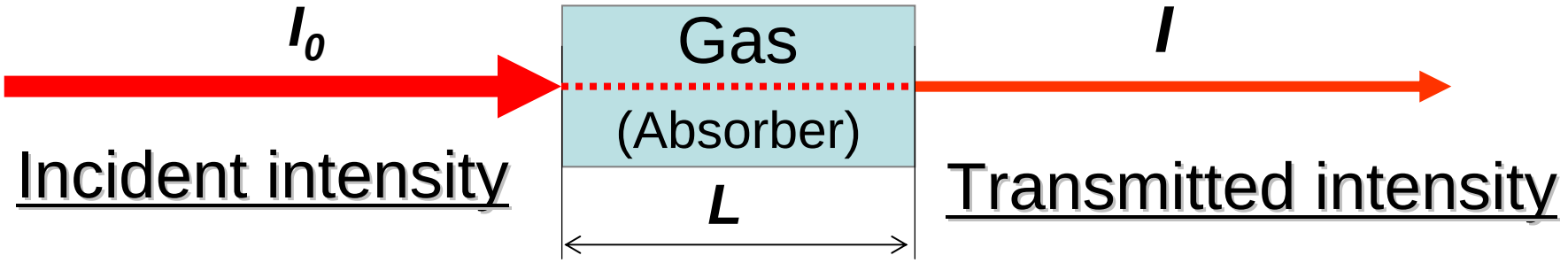

Law of Lambert-Beer

$$\log_{10}\left(\frac{I}{I_0}\right) = -\varepsilon CL$$

$\frac{I}{I_0}$: Transmissivity

ε ☐Molar absorption coefficient [cm^2/mol]

C ☐Molar concentration [mol/cm^3]

L ☐Measurement length [cm]

Light source : Infrared light source

CO_2 have absorption band around 4.3μm

Infrared absorption method

CO_2 300K 2-5μm

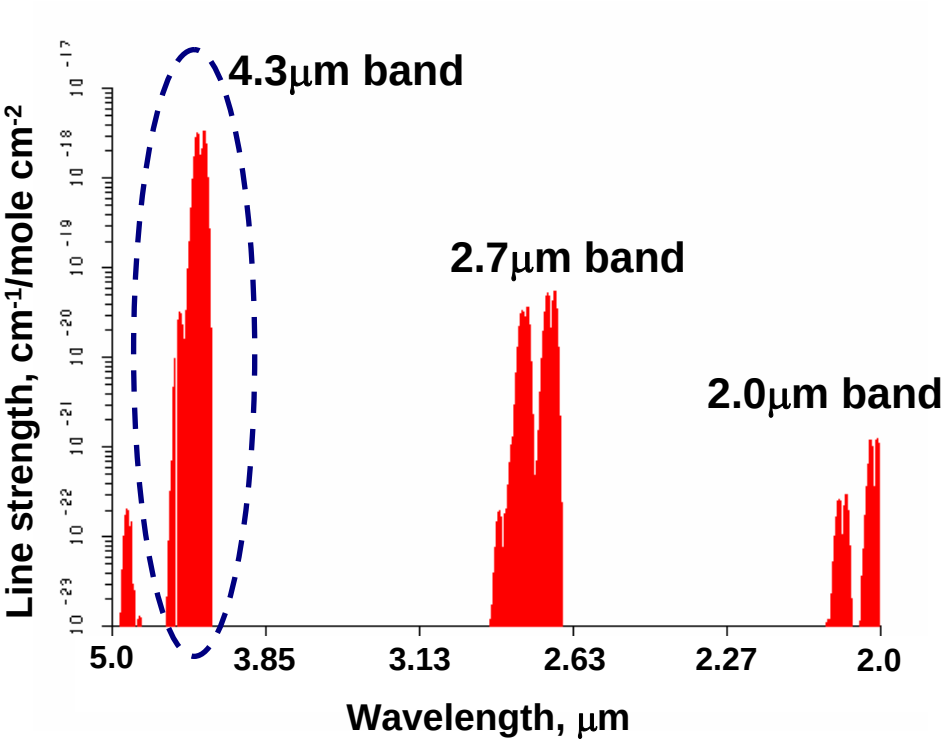

CO_2 900K 2-5μm

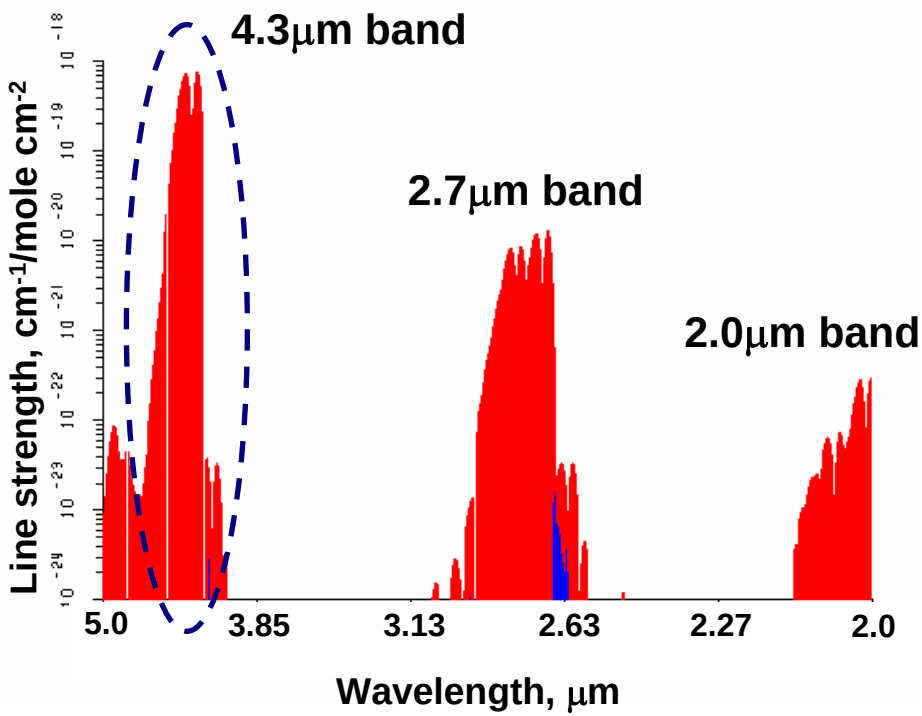

Absorption band of CO_2 (2-5μm)(HITRAN)

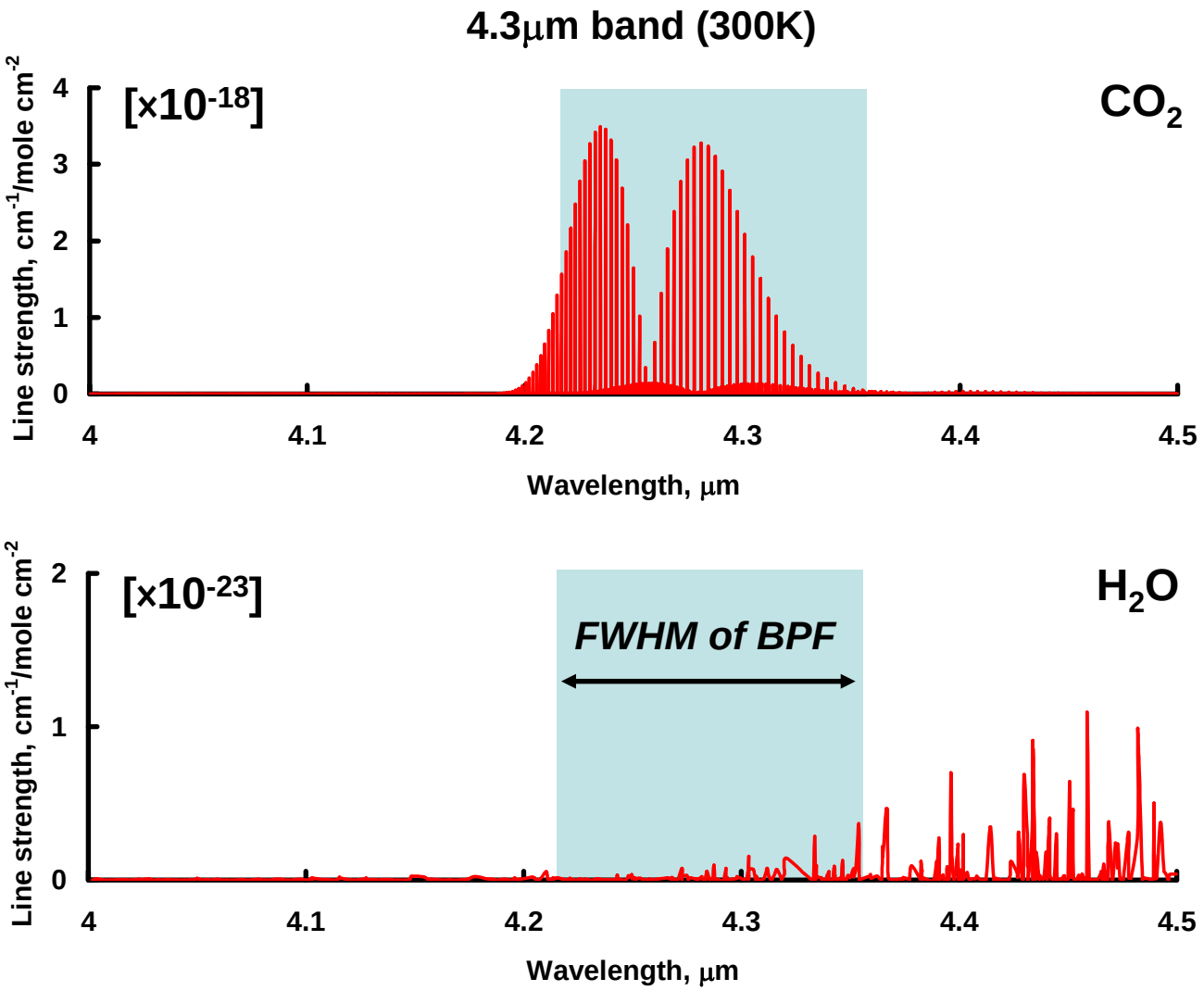

Absorbance line strength CO_2 and H_2O (4.3μm band)

- Selection of absorption lines of CO_2
  (HITRAN database)

- Absorption characteristics of CO_2
  (Effect of ambient pressure and temperature)
  (constant volume vessel)

- Developed system with spark plug sensor
  applied to a compression-expansion machine
  and to a port-injected SI engine

Contents

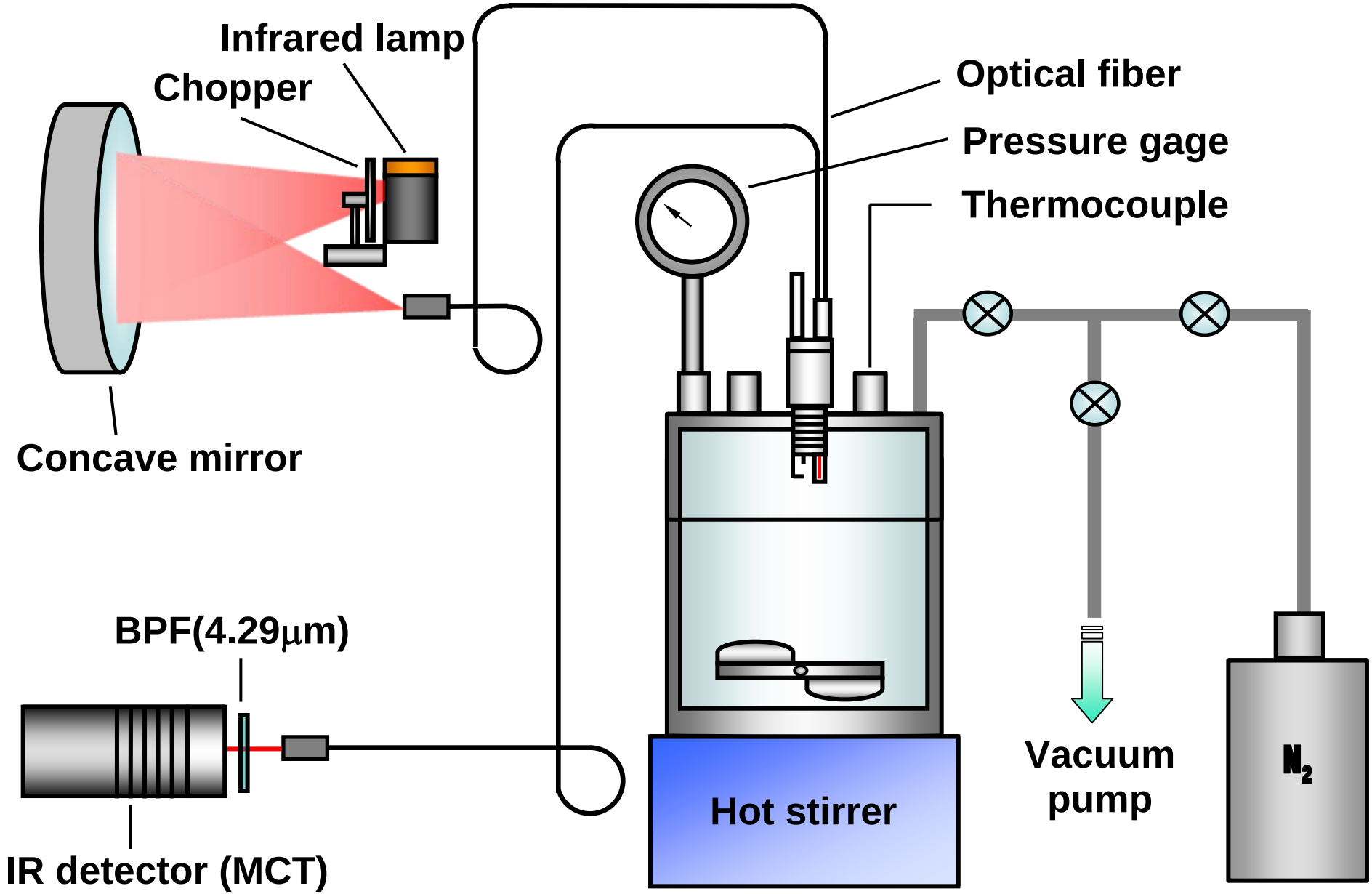

Experimental setup

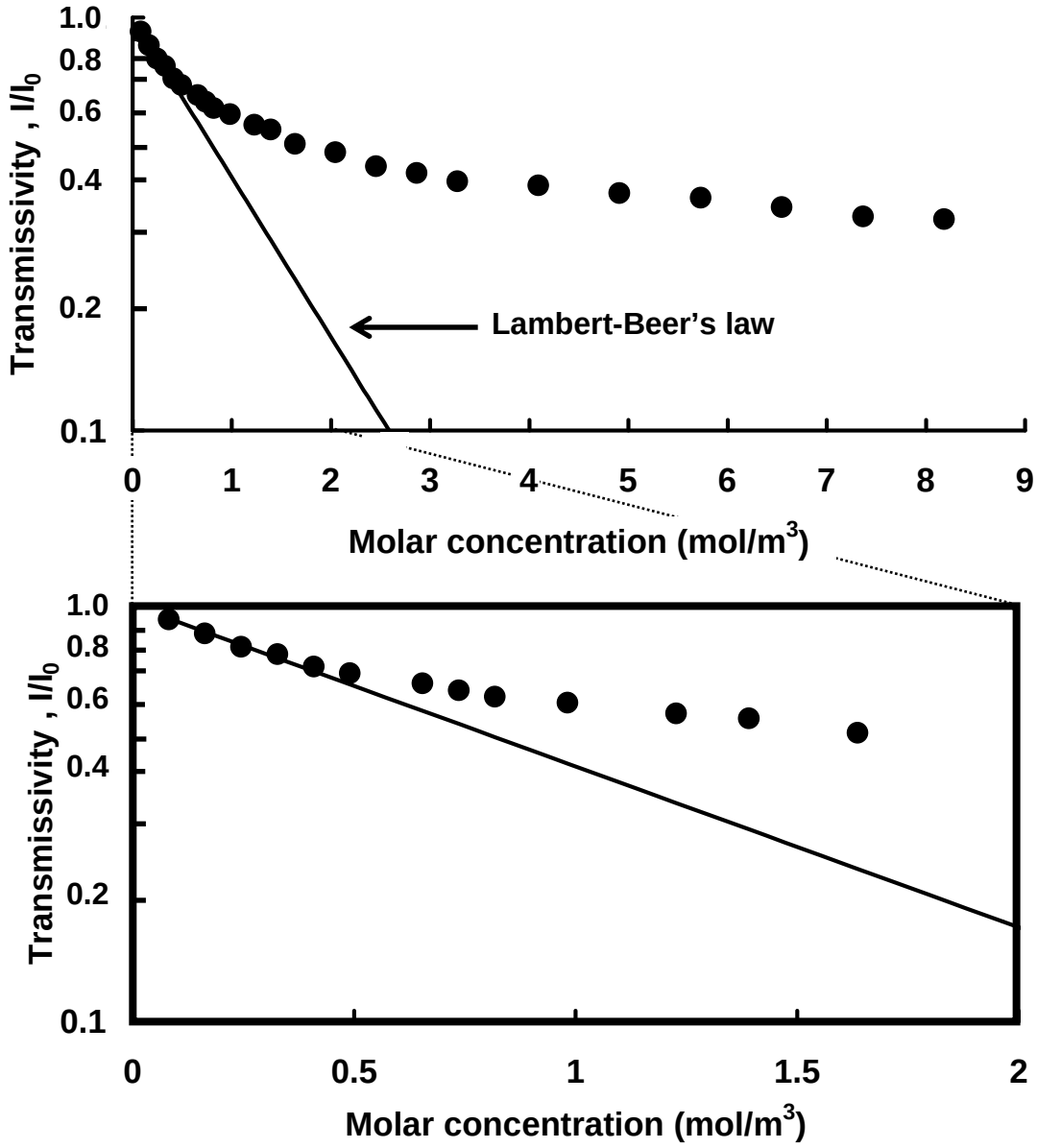

Applicability of Lambert-Beer's law

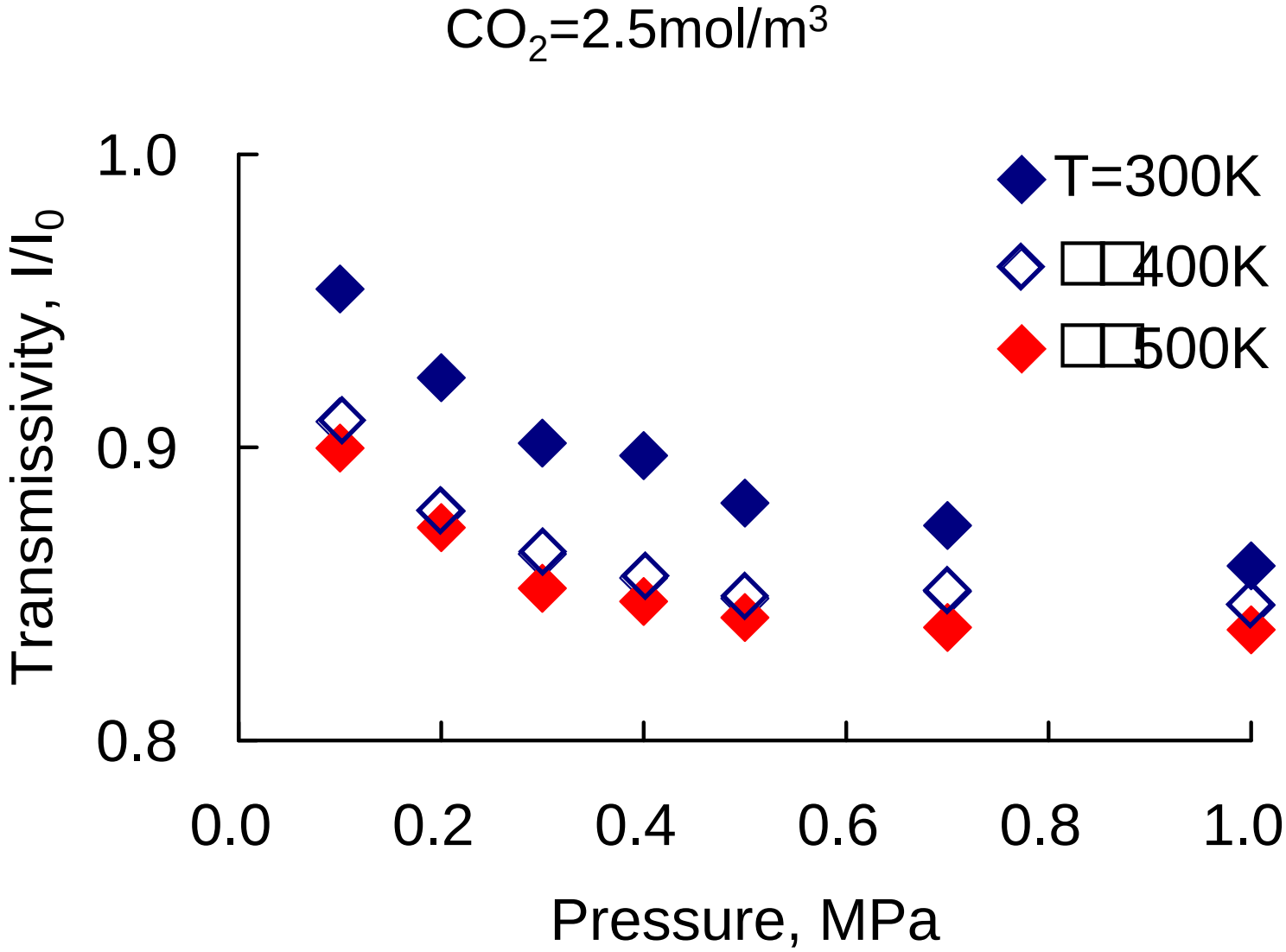

Absorption characteristics of CO_2

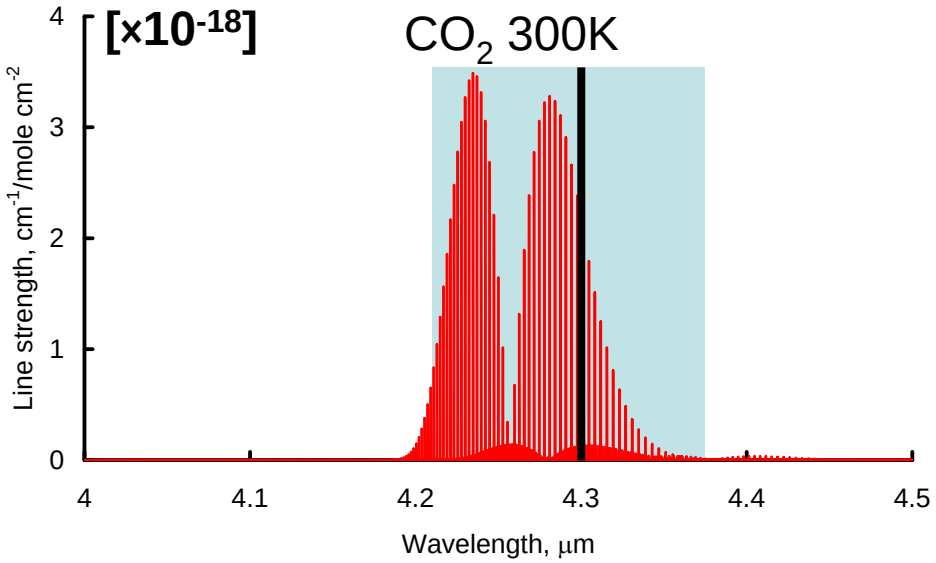

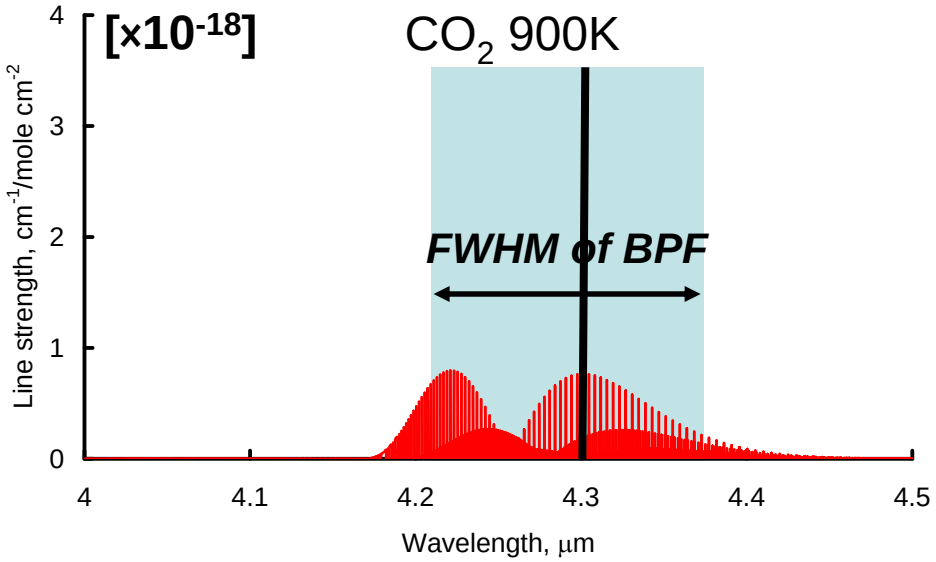

Pressure and temperature dependence of absorbance are different in each absorbance line

Problems

- *Broad-band infrared light source*
- *Band pass filter*

Effects of pressure and temperature on CO_2 concentration are needed for quantitative estimation.

Absorption characteristics of CO_2

- Selection of absorption lines of CO_2
  (HITRAN database)

- Absorption characteristics of CO_2
  (Effect of ambient pressure and temperature)
  (constant volume vessel)

- Developed system with spark plug sensor
  applied to a compression-expansion machine
  and to a port-injected SI engine

Contents

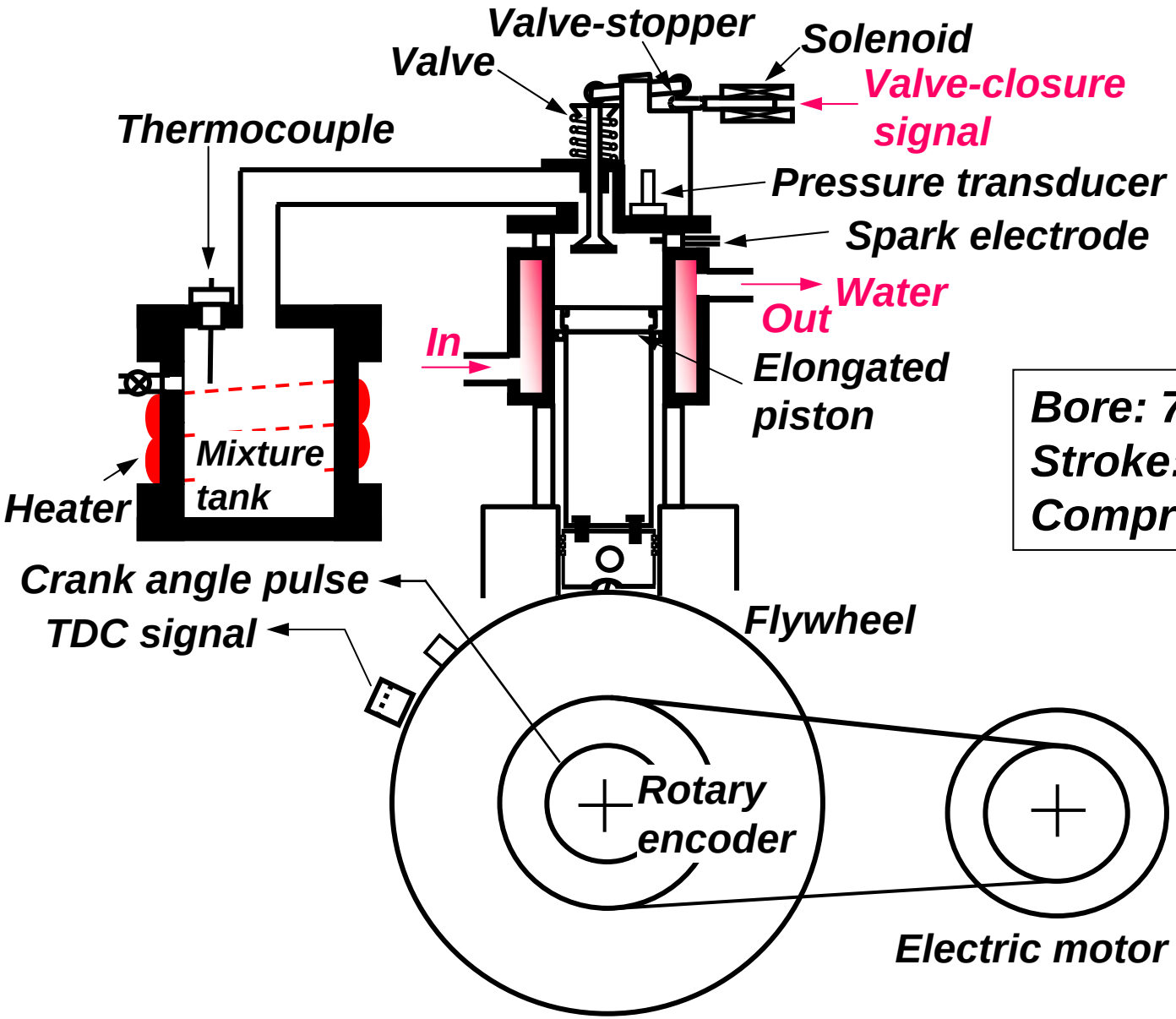

Bore: 78 mm
Stroke: 85 mm
Compression ratio: 9.02

Fuel: n-butane

θ_{ig}=10deg.BTDC

P_0=30kPa

CO2(%)

1, 3, 5, 7, 10

Compression expansion machine

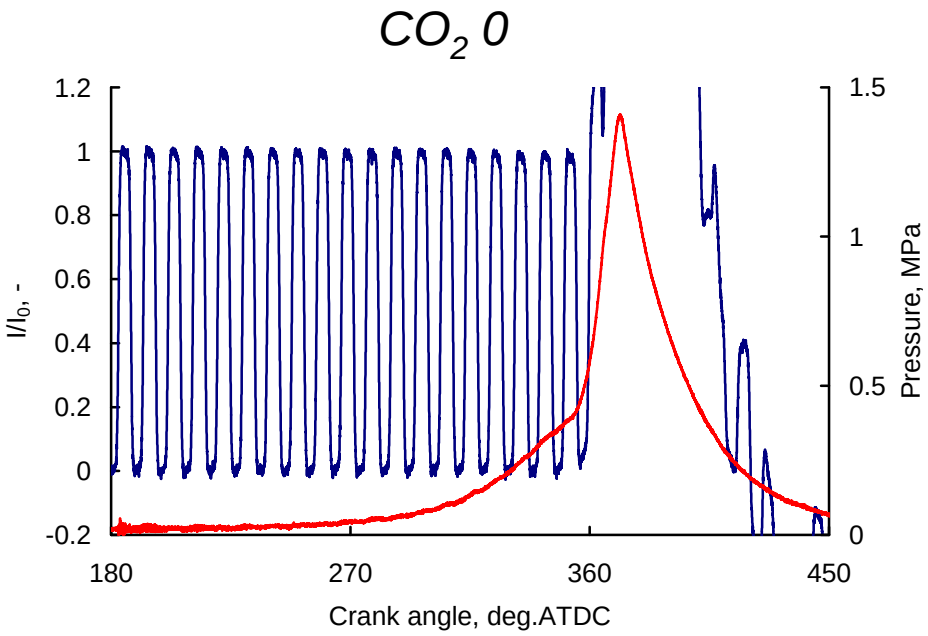

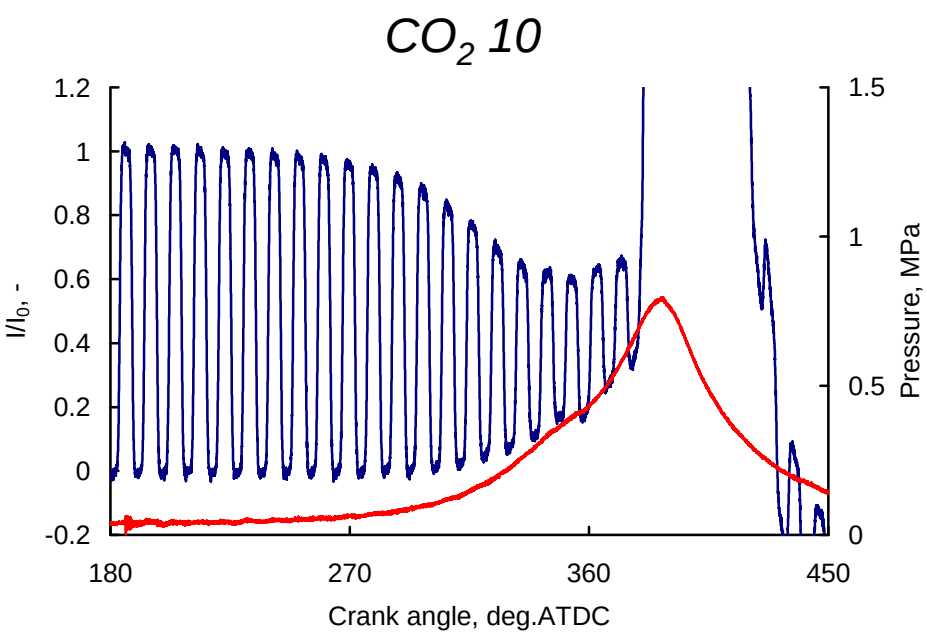

Variation of CO_2 concentration (Firing)

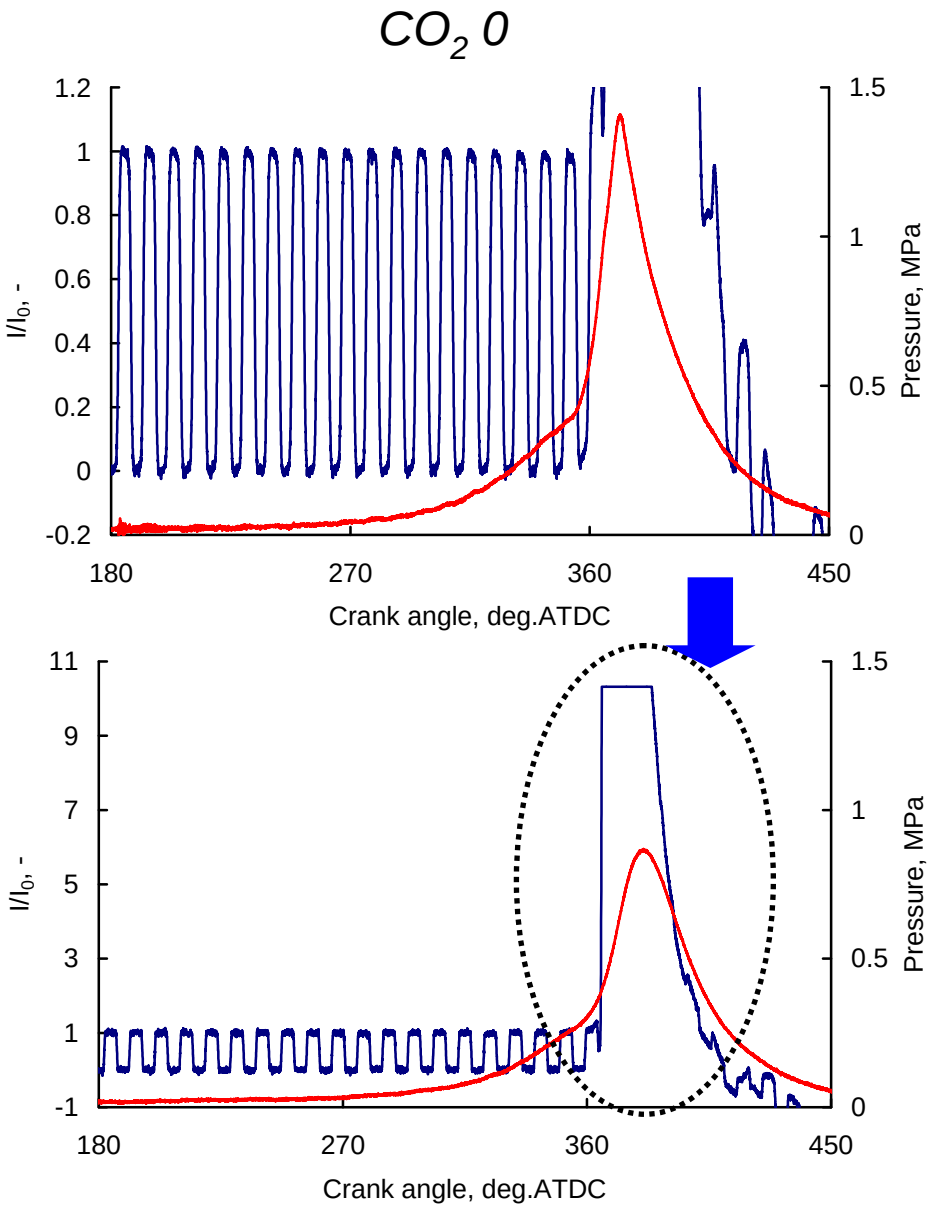

Okayama University

Variation of CO_2 concentration (Firing)

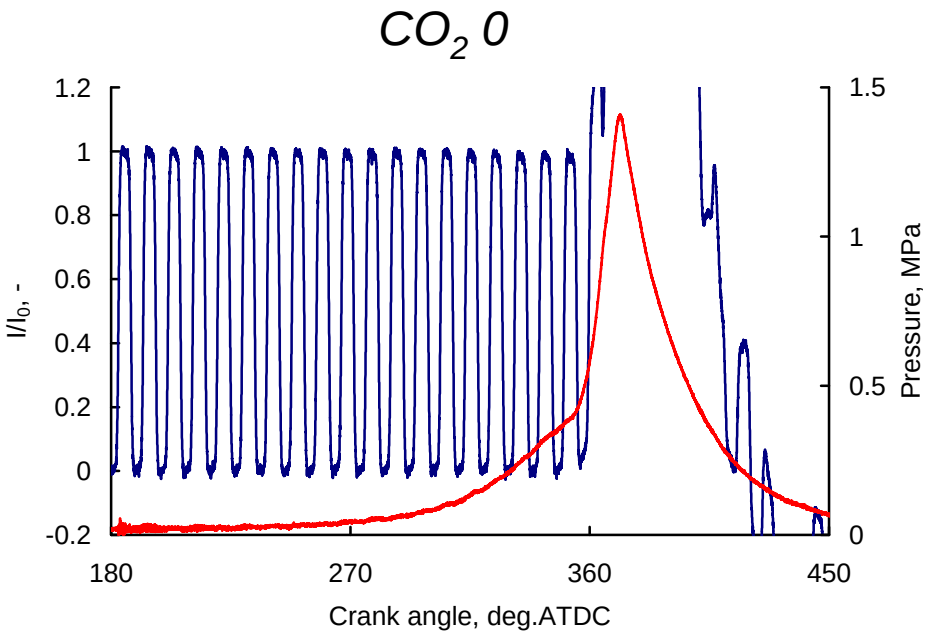

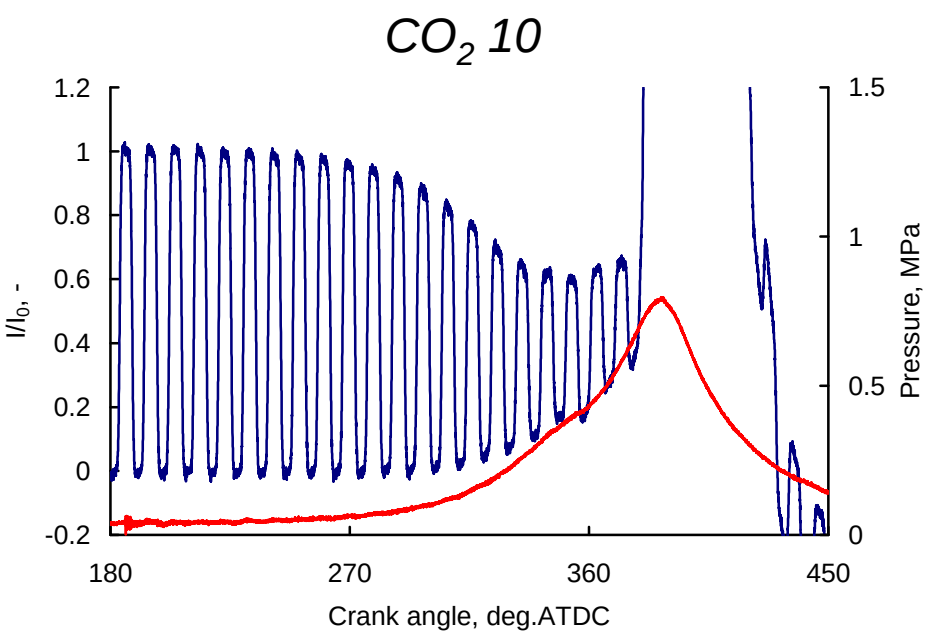

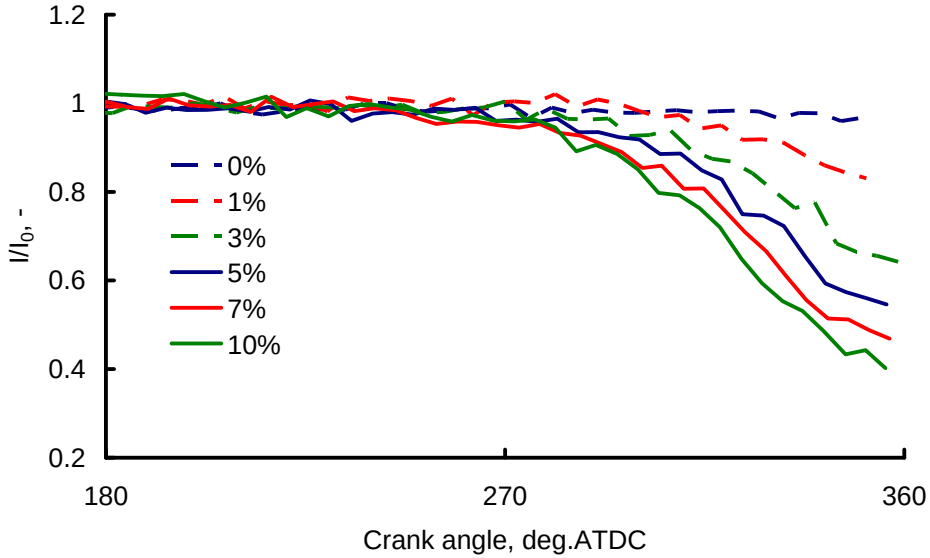

Okayama University

Variation of CO_2 concentration (Firing)

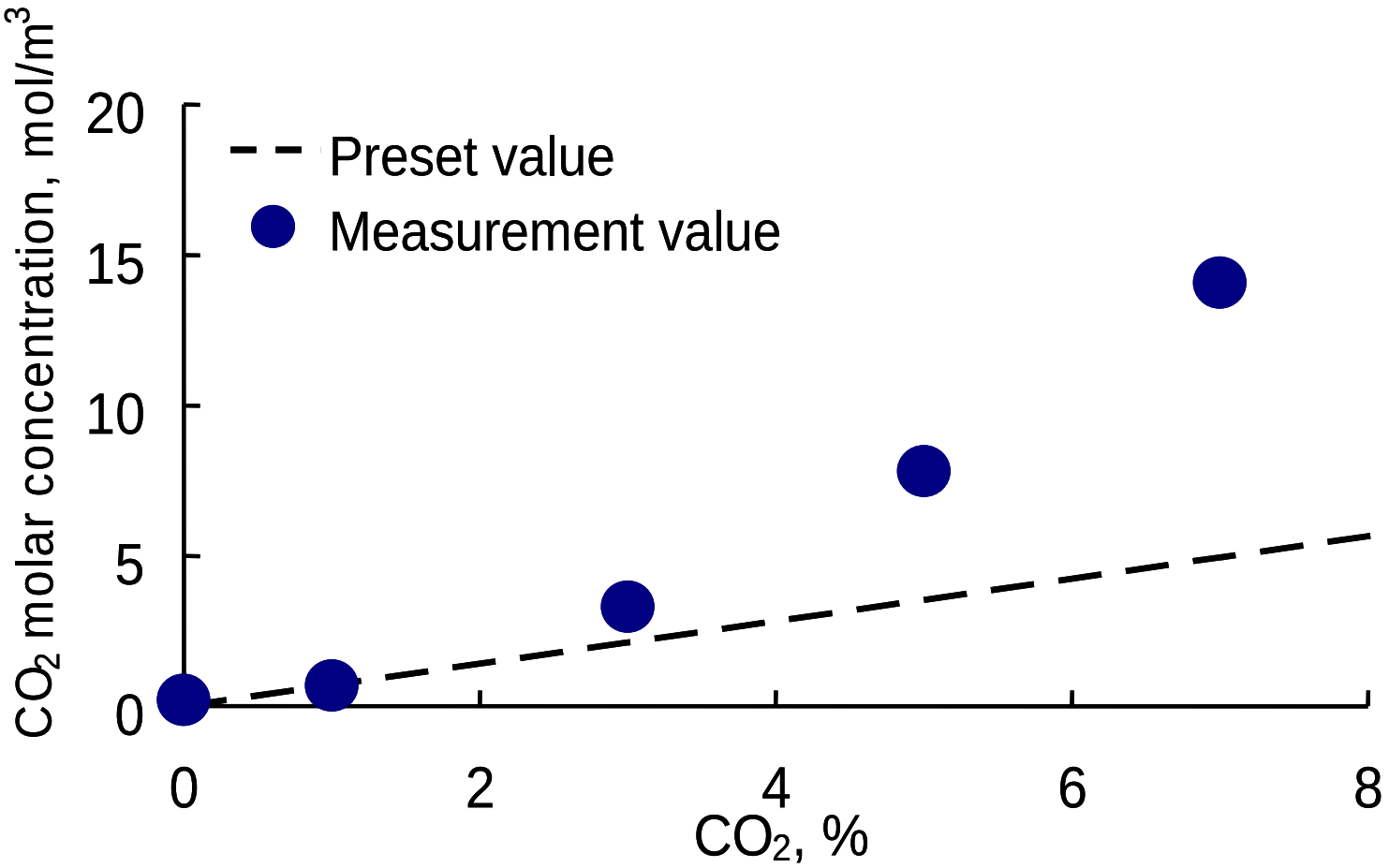

Measurements of detail pressure and temperature dependence are needed for quantitative estimation.

Molar concentration at spark timing

- Selection of absorption lines of CO_2
  (HITRAN database)

- Absorption characteristics of CO_2
  (Effect of ambient pressure and temperature)
  (constant volume vessel)

- Developed system with spark plug sensor
  applied to a compression-expansion machine
  and to a port-injected SI engine

Contents

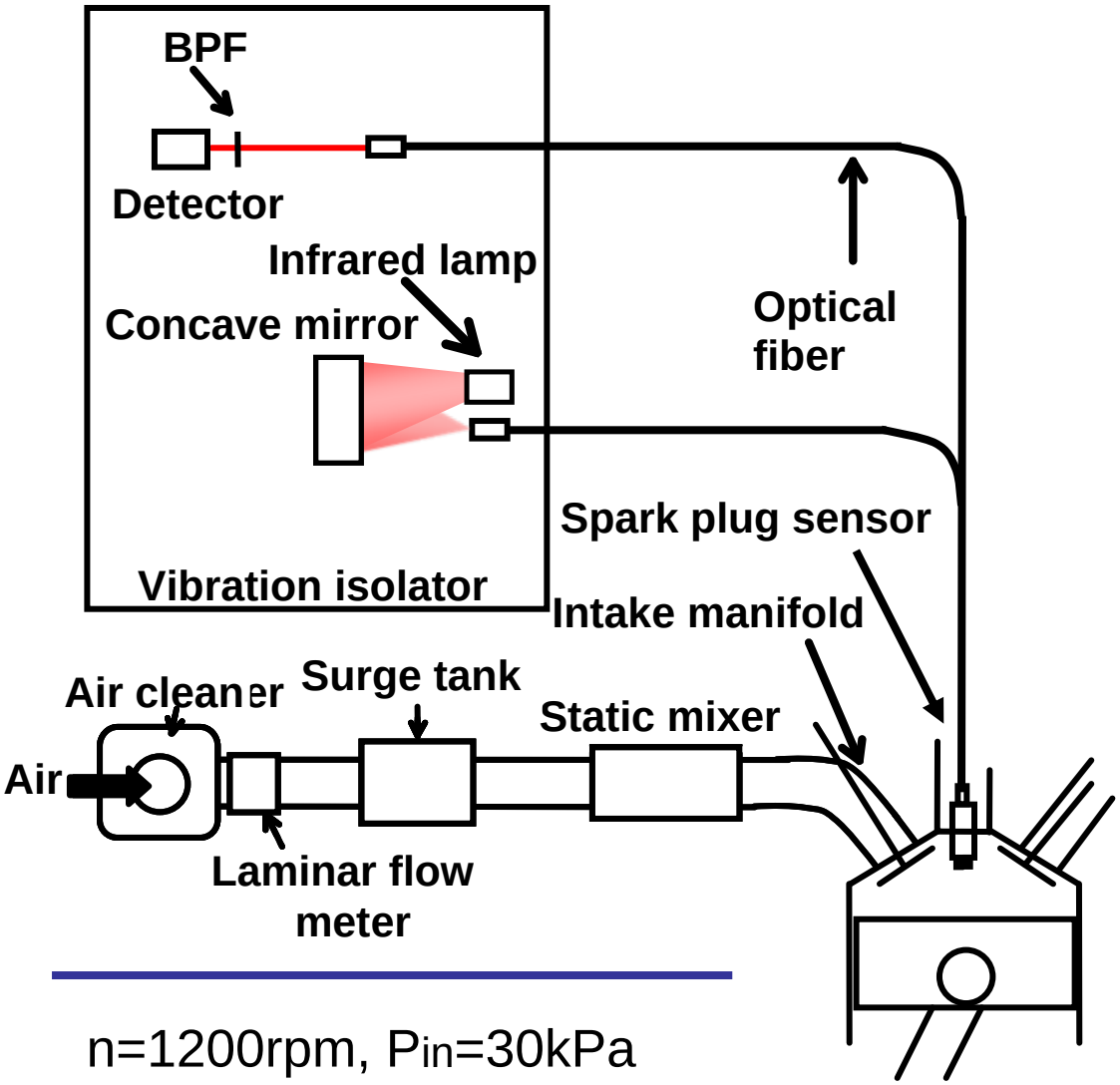

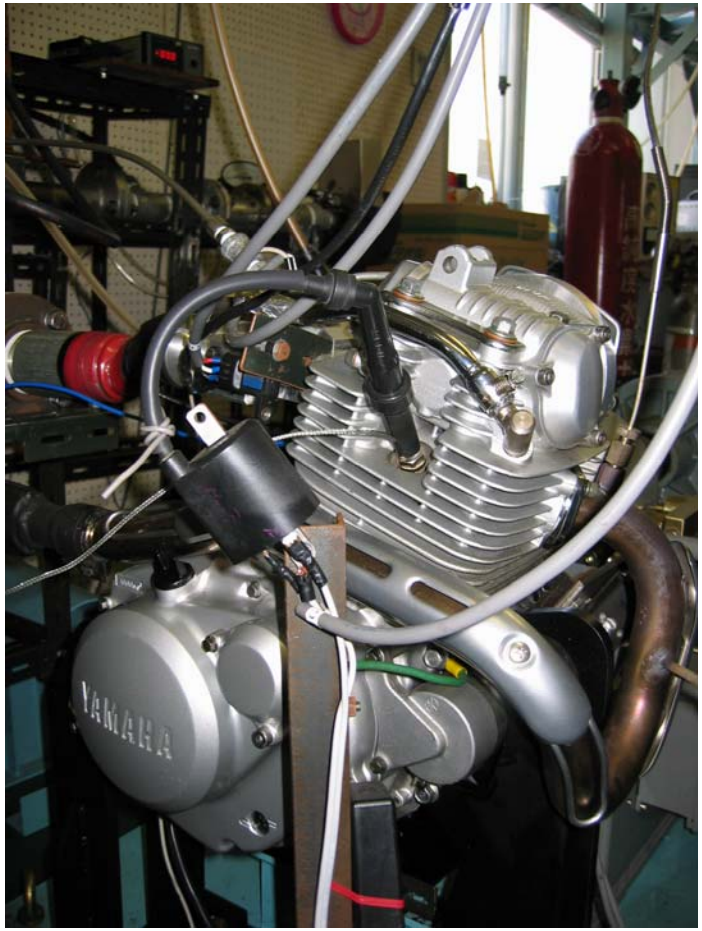

Bore x stroke: 70 x 58 mm
Compression ratio : 9.5
Single cylinder

n=1200rpm, P_{in}=30kPa

Firing (Gasoline), CO_2 (intake)=0%

Experimental setup

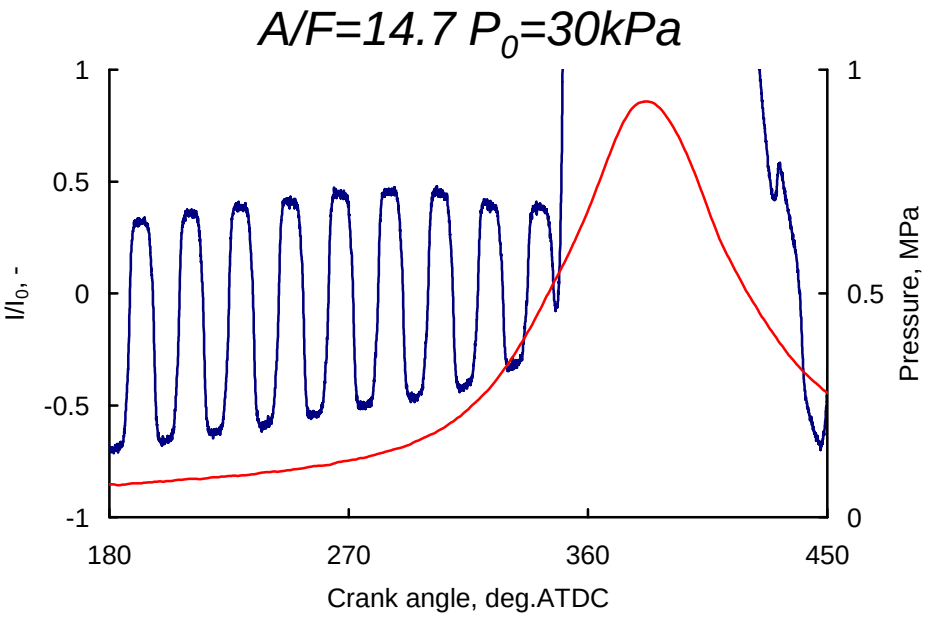

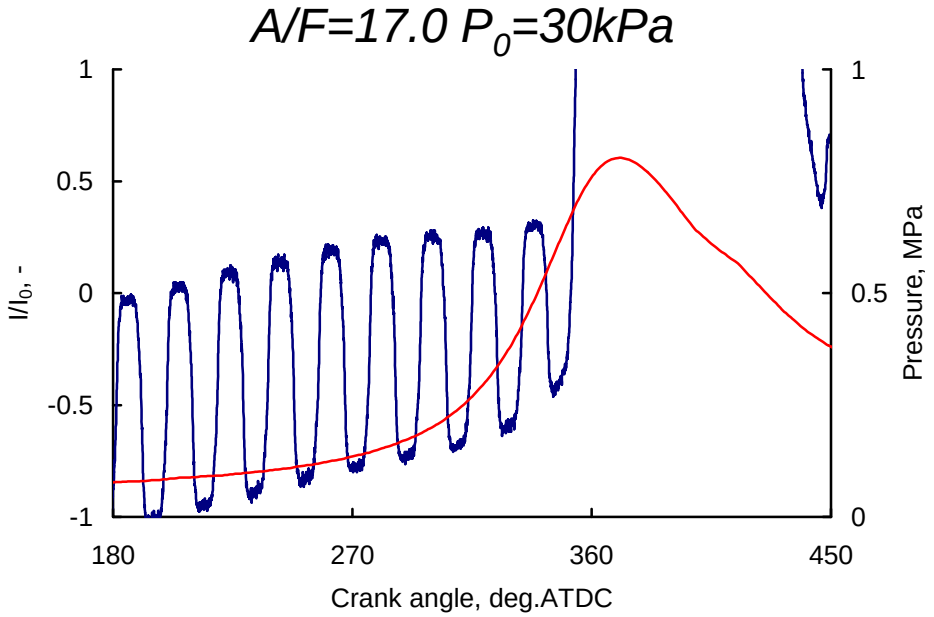

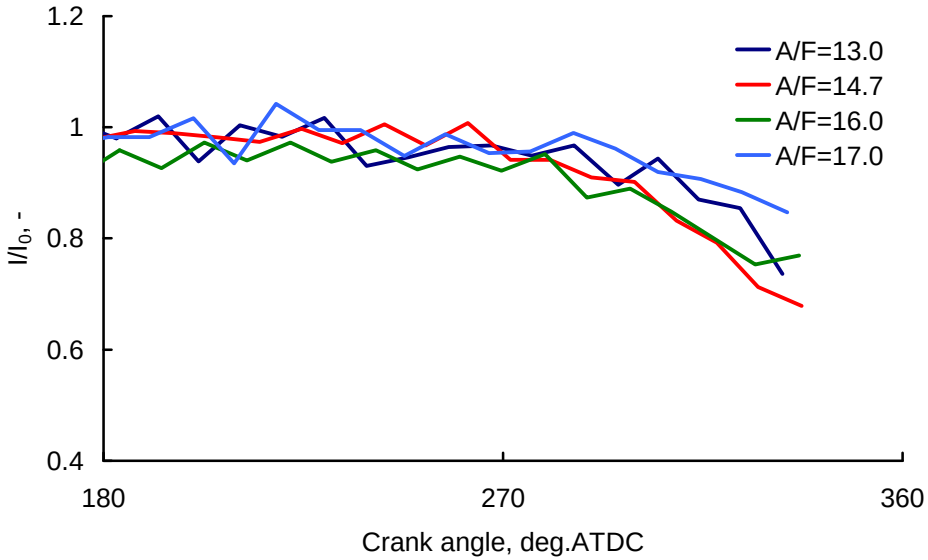

Baseline of transmissivity is not zero because of heat radiation

Absorbance under the stoichiometric condition was strong at spark timing (330deg.ATDC)

Variation of A/F (Firing)

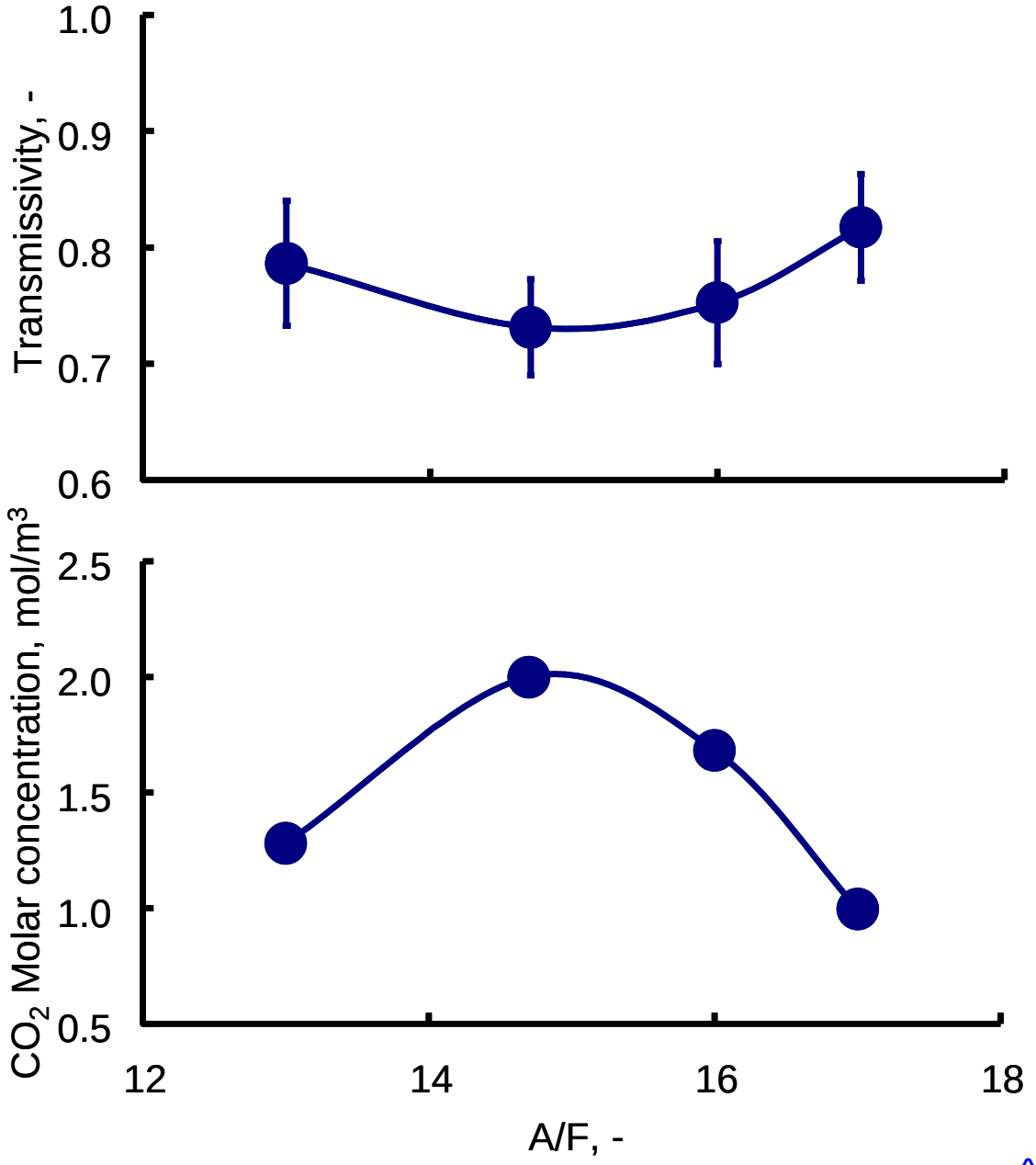

Molar concentration at spark timing

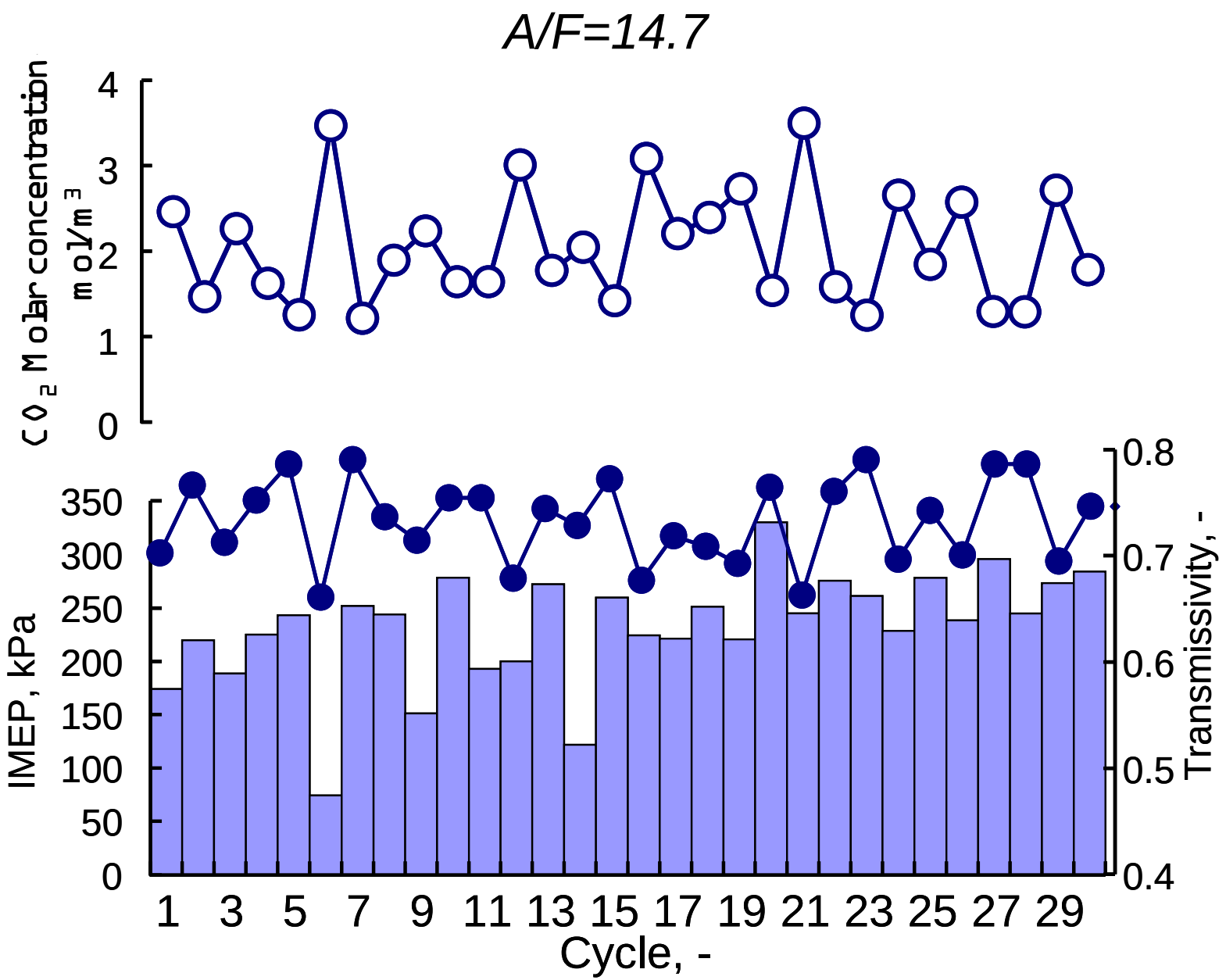

Relation between IMEP and transmissivity at spark timing

(1) We determined the relationship between the CO_2 concentration and absorption strength in advance using a constant volume vessel. Molar absorption coefficient depends on the CO_2 concentration and ambient pressure and temperature, and wavelength of absorption line.

(2) The spark plug sensor for in-situ CO_2 concentration measurement was applied to a compression-expansion machine. It was possible to qualify the CO_2 concentration inside residual gas during the compression stroke using the developed optical system with new spark plug sensor in compression-expansion machine under 3% addition of CO_2 condition.

(3) Cycle-resolved measurements were made to investigate the effects of the residual gas concentration near the spark plug on the combustion characteristics of the practical motorcycle SI engine. The system of developed measurement technique was confirmed to be valuable for cycle-to-cycle fluctuation of the CO_2 concentration around the spark plug.

Conclusions